Accepted Manuscript

A mixed hydrogeneous and hydrothermal origin of the Bahariya iron ores, Egypt: Evidences from the trace and rare earth elements geochemistry

Hassan M. Baioumy, Ahmed H. Ahmed, Mohamed Z. Khedr

PII: S0375-6742(14)00295-7
DOI: doi: 10.1016/j.gexplo.2014.08.008
Reference: GEXPLO 5446

To appear in: *Journal of Geochemical Exploration*

Received date: 13 November 2012
Accepted date: 21 August 2014

Please cite this article as: Baioumy, Hassan M., Ahmed, Ahmed H., Khedr, Mohamed Z., A mixed hydrogeneous and hydrothermal origin of the Bahariya iron ores, Egypt: Evidences from the trace and rare earth elements geochemistry, *Journal of Geochemical Exploration* (2014), doi: 10.1016/j.gexplo.2014.08.008

This is a PDF file of an unedited manuscript that has been accepted for publication. As a service to our customers we are providing this early version of the manuscript. The manuscript will undergo copyediting, typesetting, and review of the resulting proof before it is published in its final form. Please note that during the production process errors may be discovered which could affect the content, and all legal disclaimers that apply to the journal pertain.

ACCEPTED MANUSCRIPT

A mixed hydrogeneous and hydrothermal origin of the Bahariya iron ores, Egypt: Evidences from the trace and rare earth elements geochemistry

Hassan M. Baioumy[1*], Ahmed H. Ahmed[2,3], Mohamed Z. Khedr[4]

[1]*School of Physics, Universiti Sains Malaysia, 11800 USM, Penang, Malaysia*
[2]*Department of Geology, faculty of Science, Helwan University, Cairo, Egypt*
[3]*Faculty of Earth Sciences, King Abdulaziz University, Jeddah, Saudi Arabia*
[4]*Department of Geology, Faculty of Science, Kafr El Sheikh University, Egypt*

ABSTRACT

This study utilizes the trace and rare earth elements geochemistry of bulk ores and in situ LA-ICP-MS analyses of mineral grains to clarify the controversy in the origin of the Bahariya sedimentary iron ores, Egypt. Different types of iron ores were identified in the Bahariya Oasis including high grade, high-Mn, high-Ba, oolitic, and ochoreous iron ores. Hematite and goethite are the main constituents of the studied ores with some manganese oxide and hydroxide minerals (pyrolusite, bixbyite, cryptomelane, aurorite, romanechite, manjiroite, and pyrochroite). Barite is common in the high-Ba ore, while some quartz, calcite, and halite are detected in the oolitic iron ore. High-Mn iron ores are characterized by higher contents of SiO_2, Al_2O_3, MgO, CaO, Na_2O, and K_2O, while high-Ba iron ore has higher TiO_2 contents. Analyses of bulk ores and in situ mineral grains are characterized by substantially high contents of Ba (average of 9497 ppm); also Zn and Sr occur in considerably high concentrations (averages of 4263 and 429 ppm, respectively). Mn-rich ores and Mn-bearing minerals show relative enrichments of trace metals compared to the Mn-poor ores probably due to the ability of Mn-bearing minerals to fix such trace metals by adsorption, absorption, and/or replacement. The ΣREE ranges between 2.6 and 80 ppm with an average of 23 ppm. High-Mn ores show higher ΣREE (average of 61 ppm) compared with the low Mn ore (average of 13 ppm). The oolitic iron ore shows very low ΣREE

ACCEPTED MANUSCRIPT

content (7 ppm). Red and yellow ochers from El Gedida mine have similar ΣREE values (38 and 39 ppm, respectively), while red ocher from the Ghorabi area has relatively higher ΣREE (57 ppm). Chondrite-normalized REE patterns of all types of iron ores, whether in the form of bulk ores or Fe- and Mn-bearing grains, have LREE enrichment relative to HREE as shown by $(La/Yb)_N$ ratios that vary from 1.7 to 29.4. Majority of the bulk samples and mineral grains have negative Eu anomalies with Eu_N/Eu^* ranges from 0.68 to 0.8. However, bulk samples of one high grade and high-Ba ores as well as some of the Mn-bearing grains from El Gedida ores show positive Eu anomalies with Eu/Eu* ranges from 1.1 to 17.7. With few exceptions, all bulk ores and mineral grains show negative Ce anomalies with Ce/Ce* range from 0.28 to 0.96. A seawater precipitation (hydrogeneous to hydrothermal exhalite) is proposed for the Bahariya iron ores. The hydrogeneous origin is suggested based on the occurrence of high-Mn iron ores in the base of the iron ores succession, oolitic texture of some of these ores, Si-Al plot, low La/Ce ratios, high Y/Ho ratios, and LREE-enriched patterns with negative Eu anomalies of most of the bulk ores and mineral grains. The hydrothermal contribution to the source of these iron ores can be evident from the high contents of some trace elements such as Ba, Zn, and Mo, plot the analyzed samples in the hydrothermal fields of the Fe-M-(Ni+Co+Cu)*10 ternary diagram, (Co+Ni)-(As+Cu+Mo+Pb+V+Zn) and (Co+Ni+Cu-Co/Zn binary plot, low ΣREE concentrations and positive Eu anomalies and high La/Ce ratios in some of the analyzed samples. The hydrothermal contribution looks of local effect and restricted to El Gedida area.

Keywords: Iron Ores, Bahariya, Egypt, Trace Elements, Rare Earth Elements, Origin.

* Corresponding author: hassanbaioumy@hotmail.com

ACCEPTED MANUSCRIPT

1. Introduction

Economic iron ore (270 million metric tons of iron ore deposits) with an average of 47.6% Fe occur in the Bahariya Oasis (Said, 1990). The iron ores are exploited now as raw materials for the Egyptian Iron and Steel Companies, Helwan, Egypt. Due to their geological and economic significance, such deposits have been subjected to several investigations. However, the genesis of the ore has been a matter of scientific discussions for a long time. Attia (1950) and El Shazly (1962) suggested an epigenetic-supergene origin in which the deposits have been formed later than the Eocene limestone by supergene solutions. Both authors favored a deposition of leached iron in a shallow water lacustrine environment with subsequent replacement of the underlying Middle Eocene limestone. Akkad and Issawi (1963) suggested syngenetic-supergene origin where the ore deposits have been formed contemporaneously with the Eocene limestone by surface marine or fresh water in either shallow marine or lagoonal lacustrine environments. Gheith (1955), Nakhla (1961), Basta and Amer (1969) postulated an epigenetic-hypogene origin where the ore minerals were formed by metasomatic replacement by hydrothermal solutions. Tosson and Saad (1974) discussed the actual source of the iron-bearing fluids and found it to be of two types, one related to a volcanogenic source and the other derived from weathering processes. El Sharkawi et al. (1984) distinguished three genetic types for El Gedida iron ores: (1) hydrothermal–metasomatic, of a massive nature; (2) mobilized iron and manganese re-deposited in fresh water lakes, possibly through biogenic activity, cavernous, ochreous or massive in nature; and (3) a product of the weathering of glauconitic clays and sands, usually oolitic or pisolitic in texture. El Aref and Lotfy (1985) discussed the karstic significance of the iron ore deposits of Bahariya Oasis. They concluded that the ores are confined to karst features and suggested that they were formed through lateritization processes. Helba et al. (2001) recognized four depositional stages of ore development based on ironstone paragenesis suggesting

ACCEPTED MANUSCRIPT

alternating humid and dry conditions. Based on U isotopes, Dabous (2002) pointed out that the iron ore of Bahariya Oasis is neither lateritic nor volcanogenic. It is epigenetic, of fresh groundwater origin, and formed in two different stages. First, during dry climatic conditions, the iron has been oxidized and leached from the sandstone of the Nubia Aquifer by upward-moving of groundwater and deposited in the overlying pre-existing Lower-Middle Eocene karstic limestone. Second, during wet pluvial periods, the iron has been leached from the glauconitic clayey beds and infiltrated downwards and deposited on the underlying primary ore. During the two stages, initial structures, variations in pH-Eh, and biological activities were the main factors controlling the deposition and character of the ore. Baioumy and Hassan (2004) suggest that the weathering of overlying glauconites of the Hamra Formation can be the source of part of iron in the Bahariya iron ore.

Although many geochemical investigations have been performed on the iron ores from the Bahariya Oasis including major and trace elements as well as U isotopes, nothing was reported on the distributions and geochemistry of rare earth elements in these studies. In addition, the source and origin of these iron ores is still controversial as shown above. The current study shows, for the first time, the geochemistry of rare earth elements along with the trace and major elements of both bulk ores and Fe- and Mn-bearing minerals of samples represent the different iron ores including high grade, high-Ba, oolitic, high-Mn, and ocherous iron ores from El Gedida and Ghorabi areas to examine the source(s) of these deposits and clarify their origin.

2. Geology and stratigraphy of the iron ores

The Bahariya Oasis is a large depression in the Western Desert of Egypt with hot, arid climatic conditions. It is located about 270 km SW of Cairo and 180 km west of the Nile Valley (Fig. 1). Economic iron ore deposits with an average of 47.6 wt. % of Fe as Fe_2O_3 (Said, 1990) occur in

ACCEPTED MANUSCRIPT

the Bahariya Oasis. The ores are situated at the northern part of the depression and extend over an area of 11.7 km^2 with a thickness varying from 2 to 35 m, averaging 9 m (Said, 1990). The iron ores in the northern Bahariya Oasis are confined to the lower part of the Middle Eocene limestone of the Naqb Formation. The Naqb Formation ranges in thickness between 8-11.6 m and is composed of hard yellowish brown crystalline limestone with marl intercalations (El Bassyony, 2005). The iron ores occur in three areas include the Ghorabi-Nasser (3.5 km^2), El Harra (2.9 km^2), and El Gedida (15 km^2) areas. Since the current study focuses on the iron ores in the Ghorabi and El Gedida areas due to their relatively large reserves of iron ores, detailed geology and stratigraphy of these two areas will be addressed in this section.

The El Gedida iron mine is an oval shaped depression up to 15 km^2 in area, situated within the degraded cone hills of the Naqb Formation. The central part of the depression is characterized by a high relief (up to 254 m above sea level). The low Wadi area, up to 198 m above sea level, surrounds the high central area, which comprises the Cenomanian sandstone and sandy clays of the Bahariya Formation at the base, overstepped by the main Lutetian iron ore successions of Naqb Qazzun Sequence. In the Eastern and Western Wadi areas, the ore successions are truncated unconformably by late Lutetian-Bartonian glauconitic sediments with lateritic ironstone interbeds of the Hamra Formation. The iron ore sequence attains its maximum thickness, up to 35 m, in the Western and Eastern Wadi areas, and it is much reduced in the high Central area where it attains a thickness of only 11 m. This iron ore sequence consists of a pisolitic-oolitic ironstone unit followed by bedded karst iron ores intercalated with ferruginous mudstones (Fig. 2A) (e.g. El Aref et al., 1999). The thickness of the overlying glauconitic sandstone of the Hamra Formation varies in thickness from ≤ 25 m in the Western and Eastern

ACCEPTED MANUSCRIPT

Wadis areas to < 1 m in the high central area. According to Mesead and Surour (1999), the glauconite facies of El Gedida mine area represents deposition in a shallowing-upward regime.

The exposed sedimentary sequence at the Ghorabi area (Fig. 2B) starts at its bottom with the Bahariya Formation that is composed of moderately hard gray to yellowish gray clayey sediments and is overlain directly by a number of glauconitic sandstone beds range in thickness from 20 cm to 1 m and are separated by iron-rich bands and concretions. Glauconite of this horizon occurs as oval, rounded, fine to medium-grained (100 to 200 μm), moderately- to well-sorted, pale green to yellowish green pellets in smectite and iron oxides matrix (Baioumy and Bulis, 2012). This glauconite is considered by Baioumy and Bulis (2012) as parautochthonous glauconite formed from detrital smectite precursor through diffusion of K from the seawater-sediment interface in a Transgressive System Tract (TST). The total thickness of glauconite-bearing unit is approximately 4 m and is overlain by the Naqb Qazzun Sequence starting with yellowish white soft to moderately hard, laminated clayey sediments of about 3 m thick and intercalated with iron-rich bands and concretions. Overlying these yellowish white sediments, the iron ores ranging in thickness from 6 to 10 m occur as massive and brown iron ore with some reddish bands of iron ocher. Salama et al. (2012) subdivided this succession into lower and upper sequences. The lower sequence is a lagoonal manganiferous and fossiliferous ironstone facies association. The upper sequence is a peritidal microbially mediated stromatolitic and nummulitic-ooidal-oncoidal ironstone facies association. The iron ore beds are generally capped by an alluvial cover and/or quartzites of approximately 50 cm in thickness.

3. Materials and methods

Selected samples represented the different types of iron ores in the Ghorabi and El Gedida areas including high grade (Fig. 3A), oolitic (Fig. 3B), high-Mn (Fig. 3C), high-Ba (Fig. 3D), red ocher

ACCEPTED MANUSCRIPT

(Fig. 3E), and yellow ocher (Fig. 3F) iron ores were subjected to detailed petrographical, mineralogical, and geochemical investigations. Polished sections were prepared and investigated under the Olympus optical microscope (Model: BX 51). Sample powders were analyzed for their mineralogical composition using a Philips PW 1730 X-ray diffraction (XRD) technique. Operating conditions were 40 kV and 25 mA. Mineralogical and petrographical investigations were conducted at the Central Metallurgical R & D Institute (CMRDI), Cairo, Egypt.

Fused discs prepared from three bulk ore samples were analyzed for their major oxides using Philips PW 2400 X-ray fluorescence (XRF) spectrometer at Tohoku University, Japan. Tube voltage and current for W target were 40 kV and 60 mA, respectively. Loss on ignition (L.O.I.) was obtained by heating sample powders to 1000 ºC for 6 h. Trace and rare earth elements of three bulk ore samples were determined by inductively coupled plasma mass spectrometry (ICP-MS) at the ACME Lab., Canada. The sample powders were digested with 2 ml conc. HF in capped teflon bombs on an electrical hot plate (~ 150ºC) for 24 hrs. The solution was evaporated to near dryness, and re-dissolved in 2 ml 6N HNO_3 in capped teflon at 150°C for two days. The samples were then evaporated again near to dryness, then 1 ml of 6N HNO_3 was added, and the solutions were further diluted for analysis.

Major oxides as well as trace and rare earth elements concentrations of 16 mineral grains of Fe-bearing minerals (hematite and goethite) and Mn-bearing minerals (pyrolusite, bixbyite, cryptomelane, aurorite, romanechite, manjiroite, and pyrochroite) from the same bulk samples of El Gedida and Ghorabi iron ores were in-situ determined by laser-ablation (193 nm ArF excimer: MicroLas GeoLas Q-plus)-inductively coupled plasma mass spectrometry (Agilent 7500S) (LA-ICP-MS) at Kanazawa University, Japan. Analyses were performed by ablating 60-µm diameter spots. All analyses were performed at 6 Hz with energy density of 8 J/cm^2 per pulse. Details of the analytical procedures have been described by Ishida et al. (2004) and Morishita et al. (2005).

ACCEPTED MANUSCRIPT

Calibration of LA-ICP-MS analysis was carried out by using external standard as NIST 610, assuming the composition given by Pearce et al. (1997). The ^{29}Si, ^{27}Al and ^{49}Ti were used as internal standards based on SiO_2, Al_2O_3, and TiO_2 concentrations obtained by the electron microprobe. There is no differences based on these internal standard and we select calculation based on ^{29}Si. NIST 612 glass (secondary standard) was measured for quality control of each analysis. Precision or reproducibility is better than 6% for most elements, except for B, Nb, and Ta which it is better than 11-13%. The accuracy and data quality based on the reference material (NIST 612 after Pearce et al., 1997) are high for all elements except B, Nb, Ta and Hf, ranging at the 78-112% confidence level for all elements with the exception of Nb (53%), B (146%) and Ta (60%).

4. Results

4.1. Petrography and mineralogy

Microscopic investigations along with the XRD analysis indicated that hematite and goethite are the main constituents of the studied iron ores. Impurities such as Mn-bearing minerals, barite and detrital quartz occur in variable proportions in the studied ores. Hematite occurs as irregular grains and patches of variable sizes ranging from 50 to 200 μm (Fig. 4A), while goethite is characterized, in most cases, by spherical and rounded shapes of different sizes ranging from few microns up to100 μm (Fig. 4B). Detrital quartz grains are quite common in some of the studied samples and occur as relatively coarse-grained (up to 0.2 mm) subrounded and monocrystalline. Dark gray to brownish gray dull patches of variable sizes are found between grains that are most probably detrital clay minerals. Mn-bearing minerals occur either as pyrolusite or fine-grained cement-like materials (Baioumy et al., 2013). Pyrolusite occurs as relatively coarse-grained (up to

ACCEPTED MANUSCRIPT

0.1 mm) and well-crystalline between iron-bearing mineral. Manganese minerals that filled the interstitial spaces between grains appear as gray to dark gray fine-grained materials. According to Baioumy et al. (2013), the Mn-bearing minerals of these fine-grained materials are dominated by a mixture of manganese oxides and hydroxide minerals such as bixbyite, cryptomelane, aurorite, romanechite, manjiroite, and pyrochroite. In the oolitic iron ore, alternations of hematite and goethite layers form the oolitic texture of this kind of ore in El Gedid area. The ooides vary in size from very fine to coarse (Fig. 4C) with quartz and/or clayey nucleus and cemented mainly by hematite. XRD analysis of the oolitic ore indicated that this iron ore is composed of hematite, goethite, halite, and quartz. In the high-Ba ore, barite occurs as large crystals within the hematite and goethite grains (Fig. 4D). Red and yellow ochreous iron ores from the Ghorabi and El Gedida areas are composed of hematite, goethite, and traces of quartz, halite, and calcite.

4.2. Geochemistry

4.2.1. Major oxides

Concentrations of major oxides in the bulk samples as well as Fe- and Mn-bearing minerals are listed in Table 1. In El Gedida samples that represent the low Mn ores, analysis of bulk samples shows higher contents of SiO_2 and TiO_2 compared to the Fe- and Mn-bearing minerals. Al_2O_3 contents are generally higher in Mn-bearing grains compared to the Fe-bearing grains. In the Ghorabi sample that represents the high-Mn ores, analysis of the bulk samples show lower SiO_2, CaO, and K_2O contents compared to the Fe- and Mn-bearing minerals. This could be due to the presence of phases that are rich in these elements as fine-grained phases between the Fe- and Mn-bearing grains. In general, Ghorabi iron ore (high Mn) is characterized by higher contents of SiO_2, Al_2O_3, MgO, CaO, Na_2O, and K_2O compared to the El Gedida iron ores (low Mn ores). The strong positive correlations between Al_2O_3 and SiO_2, MgO, CaO, Na_2O, and K_2O (Fig. 5A)

ACCEPTED MANUSCRIPT

indicate the occurrence of these elements in association in common source with Al_2O_3 most probably as clay minerals. The oolitic iron ore from El Gedida area is characterized by relatively low Fe_2O_3 and high SiO_2 and Na_2O contents due to the relative abundance of quartz and halite, respectively. The high-Ba iron ore from El Gedida area is characterized by substantially high TiO_2 contents (2.4 wt. %) compared to other iron ores in both El Gedida and Ghorabi areas. Red ocher from the El Gedida area is characterized by lower Fe_2O_3 contents compared to the yellow ocher from the same area due to the relative abundance of goethite in the yellow ocher. The Na_2O content is higher in the red ocher compared to the yellow ocher due to the relative abundance of halite in the former. Both ochres show relatively high CaO contents, which is most probably due to the presence of calcite. Red ochre from the Ghorabi area is characterized by higher Fe_2O_3 and MnO contents compared to the ochres from El Gedida mines. It also showed relatively high SiO_2, Al_2O_3, MgO, Na_2O, and K_2O contents similar to the associated high Mn ore in the Ghorabi area. Mn-bearing minerals always have low totals due to the occurrence of these minerals as hydrous phases (e.g. Baioumy et al., 2013) as well as the relatively higher trace elements contents in these minerals.

4.2.2. Trace elements

Concentrations of trace elements in the bulk samples as well as Fe- and Mn-bearing minerals are shown in Table 2. Bulk samples and mineral grains in both Ghorabi and El Gedida areas are characterized by substantially high contents of Ba (average of 9497 ppm). Zn and Sr occur in considerably high concentrations (averages of 4263 and 429 ppm, respectively). The relatively high contents of Ba in the high-Mn deposits are due to the occurrence of Ba in the structure of Mn-bearing minerals such as romanechite (Baioumy et al., 2013). Analyses of the high Mn iron ore from the Ghorabi area show higher contents of Ba, Li, B, V, Co, Ni, Cu, Zn, Rb, Sr, Y, Zr,

ACCEPTED MANUSCRIPT

Mo, Nb, Cs, and U and less contents of As compared to that of the low Mn iron ore from the El Gedida area. The higher contents of detrital-derived elements such as Y, Nb, and Zr in the Ghorabi ores compared to those in El Gedida area as well as the positive correlations between Al_2O_3 and these elements (Fig. 5B) support the previous conclusion from the major oxide distributions that the Ghorabi area might have received more detrital inputs during their deposition compared to the El Gedida deposits. Mn-bearing minerals show considerably higher contents of Ba, Li, B, Co, Ni, Zn, Rb, Sr, Y, Zr, Mo, Nb, Cs, and U compared to the Fe-bearing minerals in both Ghorabi and El Gedida iron ores. These elements would be from solutions (seawater or hydrothermal).

Trace elements can be absorbed within the Mn-bearing minerals by a series of mechanisms including adsorption, absorption, replacement through ion exchange and co-precipitation with Mn oxides (e.g. Koschinsky and Hein, 2003; Chen et al., 2009; Randall et al., 1998). Murray (1975) and Nicholson and Eley (1997) argued that the adsorption of elements onto the surface of Mn^{4+} oxihydroxides is the main process leading to the accumulation of heavy metals in Mn deposits. Thus, the relatively higher contents of trace metals in the Mn-rich ores compared to the Fe-bearing minerals can be attributed to the ability of Mn-bearing minerals especially oxides and hydroxide phases to fix such trace metals by adsorption, absorption, and/or replacement.

4.2.3. Rare earth elements

Rare earth elements (REE) distributions in the bulk samples of different ore types as well as the Fe- and Mn-bearing grains are shown in Table 3. Except the bulk analysis of sample 14, which is characterized by significantly higher ΣREE content (80 ppm), the ΣREE contents in the bulk

ACCEPTED MANUSCRIPT

samples and mineral grains of the high grade iron ores from El Gedida iron ore (samples 14 and 15) range between 2.8 and 17.5 ppm. No difference between ΣREE contents in the Mn-bearing (average of 4.9 ppm) and Fe-bearing (average 5.9 ppm) minerals in the high grade iron ore from El Gedida area. The ΣREE contents in the bulk samples of the oolitic and high-Ba iron ores from El Gedida area are 6.7 and 9.4 ppm, respectively, which are comparable to the high grade iron ores except sample 14. Red and yellow ochres from El Gedida iron mine have almost the same ΣREE contents (ΣREE is 38.1 and 38.7 ppm, respectively), which are slightly higher than those in the bulk sample and minerals grains of the high grade, oolitic, and high-Ba iron ores except the bulk analysis of sample 14. High Mn deposits from the Ghorabi area show higher ΣREE (average 61.4 ppm) compared with the high grade (low Mn) deposits from the El Gedida area (average of 12.8 ppm). The Mn-bearing grains in this deposits show higher ΣREE (average 94.7 ppm) compared with the Fe-bearing grains (average of 28.1 ppm). The ΣREE content in the bulk red ocher from the Ghorabi area is 56.7 ppm, which is comparable to the high-Mn ores but slightly higher than the ocherous ores in El Gedida area. There is no pattern in the distribution of ΣREE between the bulk ores and those in the Fe- and Mn-bearing grains. For example, the ΣREE content in the bulk sample from El Gedida ore sample number 14 is higher than the Fe- and Mn-bearing grains, while in sample number 15 of the same deposit bulk ore has generally lower ΣREE content compared to the Fe- and Mn-bearing grains. In the Ghorabi ore, the ΣREE content in the bulk sample is lower than the ΣREE content of the Mn-bearing grains and higher than that in the Fe-bearing grains. ΣREE contents show relatively strong positive correlations (r^2= 0.7) with the Al_2O_3 contents (Fig. 5C) suggesting a detrital origin of most of these rare earth elements.

The REE patterns were chondrite-normalized using the chondrite REE values of Boynton (1984). The Eu anomaly is calculated as $E/E^*=Eu_N/(Sm_N \cdot Gd_N)$ and Ce anomaly is calculated as

ACCEPTED MANUSCRIPT

$Ce/Ce^*=(3Ce/Ce_N)/(2La/La_N+Nd/Nd_N)$. The REE patterns of the bulk ores and Fe- and Mn-bearing grains from El Gedida high grade iron ore (Fig. 6) show general light rare earth elements (LREE) enrichment relative to the heavy rare earth elements (HREE) as shown by $(La/Yb)_N$ ratios, that vary from 1.7 to 14.3. Majority of the Fe- and Mn-bearing grains as well as the bulk sample 14 show slight to intermediate negative Eu anomalies with Eu_N/Eu^* ranges from 0.68 to 0.89. However, bulk sample 15 as well as some of the Mn-bearing grains from sample number 14 and 15 show positive Eu anomalies with Eu_N/Eu^* ranges from 1.1 to 17.7. The bulk ores and mineral grains show slight to strong negative Ce anomalies with Ce_N/Ce^* ranges from 0.28 to 0.96. Oolitic iron ore from El Gedida iron mine also shows LREE enrichment over HREE ($(La/Yb)_N$= 3) with slight negative Eu anomaly (Eu/Eu*= 0.8) but pronounced negative Ce anomaly (Ce/Ce*= 0.45) (Fig. 7A). High-Ba iron ore from El Gedida area shows LREE enrichment over HREE ($(La/Yb)_N$= 14.3) with slight positive Eu anomaly (Eu/Eu*= 1.3) but pronounced negative Ce anomaly (Ce/Ce*= 0.18) (Fig. 7B). Red and yellow ochoreous iron ores from the Ghorabi and El Gedida iron ores exhibit LREE enrichment over HREE ($(La/Yb)_N$= 6-12) with slight negative Eu anomalies (Eu/Eu*= 0.6-0.9) as well as slight negative Ce anomalies (Ce/Ce*= 0.7-0.9) (Fig. 7C). The REE patterns of the bulk ores and Fe- and Mn-bearing grains from the Ghorabi high-Mn iron ore (Fig. 8) exhibit a general LREE enrichment relative to HREE as shown by $(La/Yb)_N$ ratios, that vary from 1.7 to 11.6. All analyzed samples from the Ghorabi iron ores show slight to intermediate negative Eu anomaly (Eu/Eu*= 0.73-0.90) with slight negative to slight positive Ce anomalies (Eu/Eu*= 0.8-1.20).

5. Discussion

The origin and source of iron in the Bahariya iron ores have been a matter of scientific discussions for a long time. The source of iron in the previous literatures ranges from the

ACCEPTED MANUSCRIPT

supergene origin including direct precipitation from the seawater, weathering of the overlying glauconites, leaching of the underlying Nubia sandstones and basement rocks (e.g. El Aref and Lotfy, 1985; Hussein, 1990, Dabous, 2002, Baioumy and Hassan, 2004) to hypogene origin including volcanic and hydrothermal sources (e.g. El Sharkawi et al., 1984; Tosson and Saad, 1974). This paper utilizes, for the first time, the rare earth elements geochemistry of the se deposits to examine their source and origin. Field and textural relationships as well as the major and trace elements geochemistry of the ores are also considered.

The iron ores in the Bahariya Oasis are locally oolitic and manganiferous. Assuming that this oolitic texture formed as direct precipitation of iron-rich minerals on suspended nuclei (e.g. Hemingway, 974), the occurrence of some of these iron ores in oolitic texture can suggest a hydrogeneous origin of these ores. The occurrence of high-Mn iron ores in the base of the iron ores succession of the Bahariya Oasis overlain by the low-Mn iron ores (e.g. Salama et al. 2012; Baioumy et al., 2013) suggest a descending solution as a source of Mn and Fe in the studied deposits due to the higher solubility of Mn compared to Fe and can be retained in the solution for long time until to be precipitated later between the already formed Fe-bearing minerals (e.g. Krauskopf, 1957; Nicholson, 1992; Hein et al., 2008; Mohapatra et al., 2009). In consistent with this, the occurrence of Mn-bearing minerals as cement between Fe-bearing minerals (Baioumy et al., 2013) indicates a precipitation of the former after the formation of the later due to the relatively higher solubility of Mn compared to Fe. Manganese has much greater mobility under reducing conditions in marine and lacustrine sediments (Lynn and Bonatti, 1965; Pedersen and Price, 1982), and Mn reduction and mobilization occur before Fe reduction (Sawlan and Murray, 1983). Thus, the reducing environment of the sediment permitted mobilization of Mn while Fe remained fixed, a situation that is favored in hemipelagic sediments (Hein and Koski, 1987). Thus the manganiferous horizons in the Bahariya iron ores represent more reducing depositional

ACCEPTED MANUSCRIPT

environment compared to the Mn-poor iron ores probably in a hemipelagic setting. Rare earth elements geochemistry as well as sulfur and strontium isotopes suggested a sedimentary origin of the barite associate the iron ores in El Gedida mine (Baioumy and Shinjo, in preparation). Therefore, the field relations and petrography of the iron ores and their impurities suggest a hydrogeneous origin of these ores.

Major oxide analyses of both bulk samples and Fe- and Mn-bearing minerals of the same samples suggest a hydrogeneous origin of the studied deposits through their plotting in the hydrogeneous field of the Si-Al discrimination diagram of Choi and Hariya (1992) (Fig. 9). The higher Al_2O_3 contents in Mn-bearing grains compared to the Fe-bearing grains indicates the co-genetic relationship between the Mn and Al in the Bahariya iron ores. Assuming that Al_2O_3 represents the detrital fraction of sedimentary rocks (e.g. Murray et al., 1992), the higher contents of Al_2O_3 in the Ghorabi iron ore compared to the El Gedida ore could suggest more detrital input to the depositional site of the former compared to the later. The glauconites of the Bahariya Formation underlying the iron ores in the Ghorabi area, which is highly weathered (Baioumy and Bulis, 2012) could be the source of relative Al-enrichment in these deposits. This in turns suggests a role of these glauconites as a possible source of iron for the Bahariya iron ores.

The remarkably high amount of some elements, such as Pb, Zn, Cu, and to a lesser extent, Cd, Mo, and Ba, provides evidence on the genetic role of hydrothermal solutions (Nicholson, 1992). Some of the elements are used to differentiate between Fe-Mn deposits formed in fresh water, shallow-marine and marine environments, whereas others distinguish between deposits formed under surface conditions and those precipitated at deeper levels. The Fe-Mn-(Ni+Co+Cu)*10 ternary diagram of Bonatti et al. (1972), the (Co+Ni)-(As+Cu+Mo+Pb+V+Zn) binary diagram of Nicholson (1992), and the Co+Ni+Cu versus Co/Zn binary plot of Toth (1980) are widely used to discriminate between oceanic hydrogenous and hydrothermal exhalative

ACCEPTED MANUSCRIPT

sediments. It has been found that hydrothermal deposits are depleted in Co, Ni and Cu, while they are enriched in other hydrothermal elements such as Zn, Pb, Mo, V, and As relative to hydrogenous deposits. For example, the association Mn-Ba-As-Ag is characteristic to the Mn oxides associated with either sediment-hosted exhalative or hot-spring sources (Hewett et al., 1963; Nicholson, 1992; Boyd and Scott, 1999). The high concentrations of Ba, Zn, and Mo in both bulk ores and mineral grains of the Bahariya iron ores could suggest a hydrothermal source of these ores. This is also can be seen from the plotting of all data within the hydrothermal field in the Fe-Mn-(Ni+Co+Cu)*10 ternary diagram of Bonatti et al. (1972), the (Co+Ni)-(As+Cu+Mo+Pb+V+Zn) binary diagram of Nicholson (1992), and the Co+Ni+Cu (ppm) versus Co/Zn binary plot of Toth (1980) (Fig. 10 A, B, C, respectively).

As to the rare earth elements, hydrogenous deposits show high ΣREE, while the ΣREE of hydrothermal deposits are significantly lower (Hein et al., 1990; Usui and Someya, 1997). In this regard the Bahariya iron ores have significantly low ΣREE both in the bulk ores (average of 40 ppm) and in the mineral grains (average of 42 ppm). This low concentration of ΣREE is characteristic of hydrothermal source of the studied ores.

According to Nath et al. (1997), hydrothermal crusts have La/Ce ratios similar to sea water (~2.8), while hydrogenous Mn-Fe crusts have a much lower La/Ce ratio (~0.25). The average of La/Ce ratios in the bulk samples from the Bahariya iron ores is 0.5, while the average of La/Ce ratios in the mineral grains is 0.47, which is very close to the hydrogenous Mn-Fe crusts (0.25). This supports the conclusion of major elements about the hydrogeneous origin of the studied ores. Exception is the bulk sample of the high-Ba ore that has La/Ce ratio of 3.1. Furthermore, hydrothermal solutions have a near chondritic Y/Ho ratio (27), while that for seawater is superchondritic (Bau and Dulski, 1999). The average Y/Ho ratio of the Bahariya iron

ACCEPTED MANUSCRIPT

ores is 94, which is highly enriched compared to the hydrothermal solution and could suggest a hydrogeneous source of the studied ores.

Hydrothermal solutions from the Mid-Atlantic Ridge (MAR) and East Pacific Rise (EPR) are characterized by LREE-enriched patterns with strongly positive Eu anomalies (Michard et al., 1983; Michard and Albarede, 1986; Bau and Dulski, 1999; Douville et al., 1999), whereas seawater displays HREE-enriched patterns with negative Ce anomalies (Elderfield and Greaves, 1982; Bau et al., 1996; Alibo and Nozaki, 1999). According to Michard et al., (1983), Mitra et al., (1994), Douville et al., 1999), hydrothermal solutions are produced by both high-temperature (>300 °C) and low-temperature (<200 °C) hydrothermal alteration of the oceanic crust. High-temperature hydrothermal alteration produces fluids with a pronounced positive Eu anomaly; whereas fluids produced by low-temperature hydrothermal alteration have a weak or no Eu anomaly (Michard et al., 1993). LREE-enriched patterns in all analyses of the studied ores as well as the positive Eu anomalies in some grains from El Gedida deposits may suggest a contribution from a hydrothermal source. The pronounced positive Eu anomalies in these grains (Eu_N/Eu^*= 1.1-17.7) may suggest a high-temperature hydrothermal solution (>300 °C). On the other hand, the negative Ce anomalies in almost all analyses may suggest a seawater source of the studied ores.

The direct precipitation of the studied iron ores (hydrogeneous) requires high Fe in the seawater although the dissolved of Fe in the sweater is too low (~ 4 ppb). The high dissolved Fe contents in the sweater during the precipitation of Bahariya iron ores could be due to the submarine weathering of the underlying Cenomanian glauconites that were reported in the upper part of the Bahariya Formation (e.g. Baioumy and Bulis, 2012). The submarine alteration of sedimentary rocks including Fe-rich sediments as a possible source of iron was considered in previous literatures (e.g. Hocking et al., 2010; Salama et al. 2012). The detrital iron that resulted

ACCEPTED MANUSCRIPT

from the weathering of adjacent continental masses can be also a possible source to the seawater. The positive correlations between many of the major, trace, and rare earth elements and Al_2O_3 contents suggest a detrital input during the formation of the studied iron ores and support the role of detriatal Fe to the budget of dissolved Fe in the seawater. Abundance of shales and ferruginous mudstone intervals of detrital origin intercalated with the iron ores especially in the El Gedida iron ores may support this interpretation.

As a conclusion, the obtained geochemical data indicate a seawater precipitation (hydrogeneous) source of the Bahariya iron ores as indicated from the occurrence of high-Mn iron ores in the base of the iron ores succession, the oolitic texture of some of these deposits, Si-Al plot, low La/Ce ratios, high Y/Ho ratios, and LREE-enriched patterns with negative Eu anomalies of most of the studied bulk ores and mineral grains. However, there are some lines of evidences for hydrothermal signals that might contribute to the source of the studied iron ores such as the high contents of some trace elements as Ba, Zn, and Mo, plot the analyzed samples in the hydrothermal fields of the Fe-Mn-(Ni+Co+Cu)*10 ternary diagram and (Co+Ni)-(As+Cu+Mo+Pb+V+Zn) binary diagram, low ΣREE concentrations, positive Eu anomalies in some of the analyzed grains, and high La/Ce ration in the high-Ba iron ores. The hydrothermal contribution to the source of the Bahariya iron ores looks more pronounced in the El Gedida ores compared to that in the Ghorabi area as can be indicated from the lower ΣREE and the presence of positive Eu anomalies only in some of the grains in the El Gedida ores. This can be attributed to the location of hydrothermal solutions source closer to El Gedida area.

The mixed hydrothermal and hydrogeneous sources of the iron ores were reported in the literature. Bau and Dulski (1996) and Bolhar et al. (2005) suggested that HREE-enrichment and positive Y anomalies are signals inherited from marine surface water, while positive Eu

ACCEPTED MANUSCRIPT

anomalies are signals inherited from marine bottom water through the contribution of hydrothermal solutions of the iron ores in South Africa and Australia, respectively. Also Basta et al. (2011) indicated that the REE patterns of the Wadi Karim and Um Anab banned iron formations bear the characteristics of both hydrothermal solutions and seawater. Example from the Phanerozoic iron ores, Dechomets (1985) proposed that hydrothermal fluids of dominant marine origin scavenged Fe from host rocks for the Late-Alpine iron-bearing deposits in Tuscany

6. Conclusions

Representative samples of bulk ores and Fe- and Mn-bearing minerals of different iron ore types from the Ghorabi and El Gedida areas of the Bahariya Oasis were analyzed for their major, trace, and rare earth elements to clarify the origin of these ores. The results suggested a seawater precipitation (hydrogenous to hydrothermal exhalite) of the Bahariya iron ores. Occurrence of high-Mn iron ores in the base of the iron ores succession and oolitic texture of some of these ores suggest their hydrogeneous origin. Major elements analysis supports this interpretation through the plot of all data in the hydrogeneous field of Al-Si discrimination diagram. On the other hand, the high trace elements such as Ba, Zn, and Mo and the plot of both bulk ores and Fe- and Mn-bearing minerals of different deposits in the Fe-Mn-(Ni+Co+Cu)*10 ternary diagram, (Co+Ni)-(As+Cu+Mo+Pb+V+Zn) binary diagram, and Co+Ni+Cu versus Co/Zn binary plot suggest a hydrothermal origin of the ores. The REE show lines of evidence for both the hydrogeneous and hydrothermal origin. Low La/Ce ratios, high Y/Ho ratios, and LREE-enriched patterns with negative Eu anomalies of most of the studied bulk ores and mineral grains suggest hydrogeneous origin of the studied ores. However, the low ΣREE concentrations, positive Eu anomalies in some of the analyzed grains, and high La/Ce ratio in the high-Ba ore indicate a hydrothermal

ACCEPTED MANUSCRIPT

contribution to the source of the iron ores of the Bahariya Oasis. The hydrothermal contribution looks more pronounced in the El Gedida ores compared to that in the Ghorabi area. The high dissolved Fe contents in the sweater during the precipitation of Bahariya iron ores could be due to the submarine weathering of the underlying Cenomanian glauconites of the Bahariya Formation and/or detrital iron resulted from the weathering of adjacent continental masses.

Acknowledgments

Authors would like to thank Prof. S. Arai, Kanazawa University, Japan for providing the LA-ICP-MS analytical facilities. We also thank Dr. A. Tamura, Kanazawa University, for his support in the LA-ICP-MS analyses

References

Akkad, S.E., Issawi, B., 1963. Geology and iron ore deposits Bahariya Oasis. Geol. Surv. Egyp. Paper 18, pp. 300.

Alibo, D.S., Nozaki, Y., 1999. Rare earth elements in seawater: particle association, shale-normalization and Ce oxidation. Geochim. Cosmochim. Acta 63 (3–4), 363-372.

Attia, M.I., 1950. The geology of the iron-ore deposits of Egypt. Geol. Surv. Egypt, Cairo, 34 pp.

Baioumy, H. M., Khedr, M. Z., Ahmed, A. H., 2013. Mineralogy, geochemistry and origin of Mn in the high-Mn iron ores, Bahariya Oasis, Egypt. Ore Geol. Rev. 53, 63-76.

Baioumy, H., Bulis, S., 2012. Glauconites from the Bahariya Oasis: An evidence for Cenomanian marine transgression in Egypt. J. Afric. Eart. Sci. 70, 1-7.

Baioumy, H.M., Hassan, M.S., 2004. Authigenic halloysite from El-Gideda Iron Ore, Bahria Oasis, Egypt: Characterization and Origin. Clay Miner. 39, 207-217.

ACCEPTED MANUSCRIPT

Baioumy, H.M., Shinjo, R.,. Isotopic composition and origin of barite mineralization, Bahariya Oasis, Egypt and its implication for the origin of the host iron ores (Under preparation).

Basta, E., Amer, H., 1969. El Gedida Iron Ores and Their Origin, Bahariya Oases, Egypt. Econ. Geol. 64, 424-444.

Basta, F. F., Maurice, A. E., Fontbote, L., Favarger, P., 2011. Petrology and geochemistry of the banded iron formation (BIF) of Wadi Karim and Um Anab, Eastern Desert, Egypt: Implications for the origin of Neoproterozoic BIF. Precam. Res. 187, 277-292.

Bau, M., Dulski, P., 1996. Distribution of yttrium and rare-earth elements in the Penge and Kurumaniron-formations, Transvaal Supergroup, South Africa. Precam. Res. 79, 37-55.

Bau, M., Dulski, P., 1999. Comparing yttrium and rare earths in hydrothermal fluids from the Mid-Atlantic Ridge: implications for Y and REE behavior during near vent mixing and for the Y/Ho ratio of Proterozoic seawater. Chem. Geol. 155, 77-90.

Bau, M., Koschinsky, A., Dulski, P., Hein, J.R., 1996. Comparison of partitioning behaviors of yttrium, rare earth elements, and titanium between hydrogenetic marine ferromanganese crusts and seawater. Geochim. Cosmochim. Acta 60, 1709-1725.

Bolhar, R., Van Kranendonk, M.J., Kamber, B.S., 2005. A trace element study of siderite-jasper banded iron-formation in the 3.45 Ga Warrawoona Group, Pilbara Craton-Formation from hydrothermal fluids and shallow seawater. Precam. Res. 137, 93-114.

Bonatti, E., Kraemer, T., Rydell, H., 1972. Classification and genesis of submarine iron-manganese deposits. In: Horn, D. (ed.), Ferromanganese Deposits on the Ocean Floor: International Decade of Ocean Exploration. National Science Foundation, Washington, DC, 149-166.

ACCEPTED MANUSCRIPT

Boyd, T., Scott, S.D., 1999. Two-XRD-line ferrihydrite and Fe-Si-Mn oxyhydroxide mineralization from Franklin Seamount, western Woodlark Basin, Papua New Guinea. Canad. Miner. 37, 973-990.

Boynton, W.V., 1984. Geochemistry of the REE: Meteorite studies. In: Henderson (ed.) Rare earth element geochemistry, Elsevier, pp. 63-114.

Chen, Y., Pirajno, F., Li, N., Guo, D., Lai, Y., 2009b. Isotope systematics and fluid inclusion studies of the Qiyugou breccia pipe-hosted gold deposit, Qinling Orogen, Henan province, China: implications for ore genesis. Ore Geol. Rev. 35, 245-261.

Choi, J.H. and Hariya, Y., 1992. Geochemistry and Depositional Environment of Mn Oxide Deposits in the Tokoro Belt, Northeastern Hokkaido, Japan. Econ. Geol. 87, 1265-1274.

Dabous, A.A., 2002. Uranium isotopic evidence for the origin of the Bahariya iron deposits, Egypt. Ore Geol. Rev. 19, 165-186.

Dechomets, R., 1985. Sur l'origine de la pyrite et des skarns du gisement, en contexte evaporitique, de Niccioleta (Toscane, Italie). Mineral. Depos. 20, 201-210.

Douville, E., Bienvenu, P., Charlou, J.L., Donval, J.P., Fouquet, Y., Appriou, P., Gamo, T., 1999. Yttrium and rare earth elements in fluids from various deep-sea hydrothermal systems. Geochim. Cosmochim. Acta 63 (5), 627-643.

El Aref, M.M., ElSharkawi, M.A., Khalil, M.A., 1999. The geology and genesis of stratabound to stratiform Cretaceous-Eocene iron ore deposits of El Bahariya Region, Western Desert, Egypt. Proce. Int. Conf. Geol. Arab Worl. (GAW4). pp. 450-475.

El Aref, M.M., Lotfy, Z.H., 1985. Genetic karst significance of the iron ore deposits of El Bahariya Oasis, Western Desert, Egypt. Ann. Geol. Surv. Egyp. 15, 1-30.

El Bassyony, A.A., 2005. Bahariya teetotumensis n. gen. n. sp. from the Middle Eocene of Egypt. Rev. Paléobiol. Genèv. 24, 319-329.

ACCEPTED MANUSCRIPT

El Sharkawi, M.A., Higazi, M.M., Khalil, N.A., 1984. Three genetic iron ore dikes of iron ores at El Gedida mine, Western Desert. Egypt. Geol. Soc. Egypt. 21st Annual Meeting, Cairo, Egypt (Abstract).

El Shazly, E.M., 1962. Report on the results of drilling in the iron ore deposit of Gebel Ghorabi, Bahariya Oasis, Western Desert. Geol. Surv. Egyp. 25 pp.

Elderfield, H., Greaves, M.J., 1982. The rare earth elements in seawater. Natur. 296, 214-219.

Gheith, M.A., 1955. Classification and review of iron ore deposits. Symposium of Applied Geology of Near East, UNESCO, Ankara, 106-113.

Hein, J.R., and Koski, R.A., 1987. Bacterially mediated diagenetic origin for chert-hosted manganese deposits in the Franciscan Complex, California Coast Ranges. Geol. 15, 722-726.

Hein, J.R., Schulz, M.S., Dunham, R.E., Stern, R.J., Bloomer, S.H., 2008. Diffuse flow hydrothermal manganese mineralization along the active Mariana and southern Izu-Bonin arc system, western Pacific. J. Geoph. Res., 113, B08S14, doi:10.1029/2007JB005432.

Hein, J.R., Schulz, M.S., Kang, J.K., 1990. Insular and submarine ferromanganese mineralization of the Tongap-Lau region. Mar. Miner. 9, 305-354.

Helba, A. A., El Aref, M. M., Saad, F., 2001. Lutetian oncoidal and ooidal ironstone sequence; depositional setting and origin; northeast El Bahariya Depression, Western Desert, Egypt. Egypt. J. Geol. 45/1A, 325-351.

Hemingway, J.E., 1974. Jurassic. In: Raynor, D.H. and Hemingway, J.E. (eds.). The geology and mineral resources of Yorkshire. Yorkshire Geol. Soc. pp. 16l-223.

Hewett, D.F., Fleischer, M., Conklin, N., 1963. Deposits of the manganese oxides: Supplement: Econ. Geol. 58, 1-51.

ACCEPTED MANUSCRIPT

Hocking, M.W.A., Hannington, M.D., Percival, J.B., Stoffers, P., Schwarz-Schampera, U., de Ronde, C.E.J., 2010. Clay alteration of volcaniclastic material in a submarine geothermal system, Bay of Plenty, New Zealand. J. Volcan. Geoth. Res. 191, 180-192.

Hussein, A., 1990. Mineral Deposits," In: R. Said, Ed., The Geology of Egypt, Taylor and Francis Publishers, London, pp. 511-566.

Ishida, Y., Morishita, T., Arai, S., Shirasaka, M., 2004. Simultaneous in-situ multi-element analysis of minerals on thin section using LA-ICP-MS. The Science Reports of Kanazawa University 48, 31-42.

Koschinsky, A., Hein, J.R., 2003. Uptake of elements from seawater by ferromanganese crusts: solid-phase associations and seawater speciation. Mar. Geol. 198, 331-351.

Krauskopf, K.B., 1957. Separation of manganese from iron in sedimentary process. Geochim. Cosmochim. Act. 12**,** 61-84.

Lynn, D., Bonatti, E., 1965. Mobility of manganese in diagenesis of deep-sea sdiments. Mar. Geol. 3, 457-474.

Mesaed, A.A., Surour, A.A., 1999. Mineralogy and geochemistry of the Bartonian strata bound diagenetic and lateritic glauconitic ironstones of El-Gidida mine, Bahria Oasis, Egypt. Proce. Int. Conf. Geol. Arab Worl. pp. 509-540.

Michard, A., Albarède, F., 1986. The REE content of some hydrothermal fluids. Chem. Geol. 55, 51-60.

Michard, A., Albarede, F., Michard, G., Minster, J.F., Charlou, J.L., 1983. Rare-earth elements and uranium in high-temperature solutions from East Pacific Rise hydrothermal vent field (13 degrees N). Natur. 303, 795-797.

ACCEPTED MANUSCRIPT

Michard, A., Michard, G., Stuben, D., Stoffers, P., Cheminee, J.-L., Binard, N., 1993. Submarine thermal springs associated with young volcanoes: the Teahitia vents, Society islands Pacific Ocean. Geochim. Cosmochim. Acta 57, 4977-4986.

Mitra, A., Elderfield, H., Greaves, M.J., 1994. Rare earth elements in submarine hydrothermal fluids and plumes from the Mid-Atlantic Ridge. Mar. Chem. 46, 217-235

Mohapatra, B.K., Mishra, P.P., Singh, P.P., Rajeev, S., 2009. Manganese ore deposits in Koira-Noamundi province of Iron Ore Group, north Orissa, India: In the light of geochemical signature Chem. der Erd.-Geochem. 69, 377-394.

Morishita, T., Ishida, Y., Arai, S., Shirasaka, M., 2005. Determination of multiple trace element compositions in thin (< 30 μm) layers of NIST SRM 614 and 616 using laser ablation-inductively coupled plasma–mass spectrometry. Geost. Geoan. Res. 29, 107-122.

Murray, R.W., Jpnes, D.L., Buchholtz, T.B., 1992. Diagenetic formation of bedded chert: evidence from chemistry of the chert-shale couplet. Geol. 20, 271-274.

Nakhla, F.M., 1961. The iron ore deposits of El-Bahariya Oasis, Egypt. Econ. Geol. 56, 1103-1111.

Nath, B.B., Pluger, W.L., Roelandts, I., 1997. Geochemical constraints on the hydrothermal origin of ferromanganese incrustations from the Rodriguez triple junction, Indian Ocean. In: Nicholson, K., Hein, J.R., Bu¨hn, B., Dasgupta, S. (Eds.), Manganese Mineralization: Geochemistry and Mireralogy of Terrestrial and Marine Deposits. Geol. Soci. Lond. Spec. Publ. 119, 199-211.

Nicholson, K., 1992. Contrasting mineralogical-geochemical signatures of manganese oxides: guides to metallogenesis. Econ. Geol. 87, 1253-1264.

ACCEPTED MANUSCRIPT

Nicholson, K., Eley, M., 1997. Geochemistry of manganese oxides: metal adsorption in freshwater and marine environments. In: Nicholson, K., Hein, J.R., Bühn, B., Dasgupta, S. (Eds.), Manganese Mineralization: Geochemistry and Mineralogy of Terrestrial and Marine Deposits. Geol. Soci. Lond. 309-326.

Pearce, N.J.G., Perkins, W.T., Westgate, J.A., Gorton, M.P., Jackson, S.E., Neal, C.R., Chenery, S.P., 1997. A compilation of new and published major and trace element data for NIST SRM 610 and NIST SRM 612 glass reference materials. Geost. Newslet. 21, 115-144.

Pedersen, T.F., Price, N.B., 1982. The geology of manganese carbonate in Panama Basin sediments. Geochim. Cosmochim. Acta 46, 59-68.

Randall, S.R., Sherman, D.M., Ragnarsdottir, K.V., 1998. An extended X-ray absorption fine structure spectroscopy investigation of cadmium sorption on cryptomelane (KMn_8O_{16}). Chem. Geol. 15, 95-106.

Said, R., 1990. The Geology of Egypt. Elsevier, New York, 734 pp.

Salama, W., El Aref, M.M., Gaupp, R., 2012. Mineralogical and geochemical investigations of the Middle Eocene ironstones, El Bahariya Depression, Western Desert, Egypt, Gond. Res. 22, 717-736.

Sawlan, J.J., Murray, J.W., 1983. Trace elelmemnt remobilization in the interstitial waters of red clay and hemipelagic marine sediments. Ear. Planet. Sci. Lett. 64, 213-230.

Tosson, S., Saad, N.A., 1974. Genetic studies of El-Bahariya iron ore deposits, Western Desert, Egypt. Nue. Jb. Miner. Abh. 121, 317-393.

Toth, J.R., 1980. Deposition of submarine crusts rich in manganese and iron. Geol. Soci. Amer. Bull. 91, 44-54.

Usui, A., Someya, M., 1997. Distribution and composition of marine hydrogenetic and hydrothermal manganese deposits in the northwest Pacific. In: Nicholson, K., Hein, J.R.,

ACCEPTED MANUSCRIPT

Buhn, B., Dasgupta, S. (Eds.), Manganese Mineralization: Geochemistry and Mineralogy of Terrestrial and Marine Deposits. Geol. Soci. Lond. Spec. Publ. 119, 177-198.

ACCEPTED MANUSCRIPT

ACCEPTED MANUSCRIPT

Figures captions

Fig. 1: Location and geological maps of the Bahariya Oasis, Western Desert, Egypt with the location of the studied iron ores (From El Bassyony, 2005).

Fig. 2: Stratigraphic columnar section of the iron ores in the Eastern Wadi of El Gedida mine area (A) (From El Aref et al, 1999) and Ghorabi (B) areas (From Baioumy et al., 2013).

Fig. 3: Field photos of different iron ores from the Bahariya Oasis. (A) High grade iron ores from El Gedida mine. (B) Oolitic iron ores from El Gedida mine. (C) High-Mn iron ores from Ghorabi area. (D) High barite iron ores from El Gedida mine (arrow). (E) Red ocher from El Gedida mine (arrow). (F) Yellow ocher from El Gedida mine (arrow). Hammer length is approximately 20 cm.

Fig. 4: Photomicrographs of polished sections from the Bahariya iron ores. (A) Abundance of high reflectivity hematite in the high grade iron (H) that contains inclusions and small grains of brownish isotropic nonmetallic constituents (N) most probably quartz and clayey materials. (B) Spherical shaped goethite (G) grains of variable sizes that contain inclusions and small grains of brownish isotropic nonmetallic constituents (N). (C) Oolitic iron ore from El Gedida area in which oolites of variable sizes are composed of hematite (H) and goethite (G) alternations around quartz nucleus (Q) and cemented mainly by hematite (H). (D) High-Ba iron ore from El Gedida area in which coarse-grained barite (B) cemented by the Fe-bearing minerals (H) as well as isotropic nonmetallic constituents (N) of variable sizes.

Fig. 5: (A) Strong positive correlations between Al_2O_3 and major oxides (SiO_2, MgO, CaO, Na_2O, and K_2O), (B) Strong positive correlations between Al_2O_3 and the detrital trace elements (Nb, Y, and Zr), and (C) Strong positive correlations between Al_2O_3 and the ΣREE in the bulk ores and mineral grains of the studied ores.

ACCEPTED MANUSCRIPT

Fig. 6: Chondrite-normalized REE patterns for the bulk and Fe- and Mn-bearing minerals of two samples (14 and 15) represent the high grade iron ores from El Gedida mine. (A) Chondrite-normalized REE pattern for the bulk iron ore of sample number 14, (B) REE patterns for the Fe-bearing minerals of sample number 14, and (C) REE patterns for the Mn-bearing minerals of sample number 14. (D) Chondrite-normalized REE pattern for the bulk iron ore of sample number 15, (E) REE patterns for the Fe-bearing minerals sample number 15, and (F) REE patterns for the Mn-bearing minerals of sample number 15.

Fig. 7: (A) Chondrite-normalized REE patterns for the bulk oolitic iron ore from El Gedida area. (B) Chondrite-normalized REE patterns for the bulk barite-rich iron ore from El Gedida area. (C) Chondrite-normalized REE patterns for the bulk ochreous iron ores from El Gedida and Ghorabi areas.

Fig. 8: Chondrite-normalized REE patterns for the bulk high-Mn iron ores (A) as well as the Fe-bearing minerals (B) and Mn-bearing minerals (C) in the Ghorabi iron ores.

Fig. 9: Si-Al discrimination diagram of Choi and Hariya (1992). XRF data of bulk samples as well as the LA-ICP-MS data of Fe- and Mn-bearing minerals of all samples from El Gedida and Ghorabi areas plotted in the field of hydrogeneous manganese deposits.

Fig. 10: Plot of the Bahariya iron ores in the triangular diagram of (Ni+Co+Cu)*10-Mn-Fe (Bonatti et al., 1972) (A), (Ni+Co) versus (As+Cu+Mo+V+Zn) discrimination diagram (Nicholson, 1992) (B), and (Co+Ni+Cu) versus Co/Zn binary plot of Toth (1980) (C). The studied iron ores plotted in the field of hydrothermal origin in all these diagrams.

ACCEPTED MANUSCRIPT

Figure 1

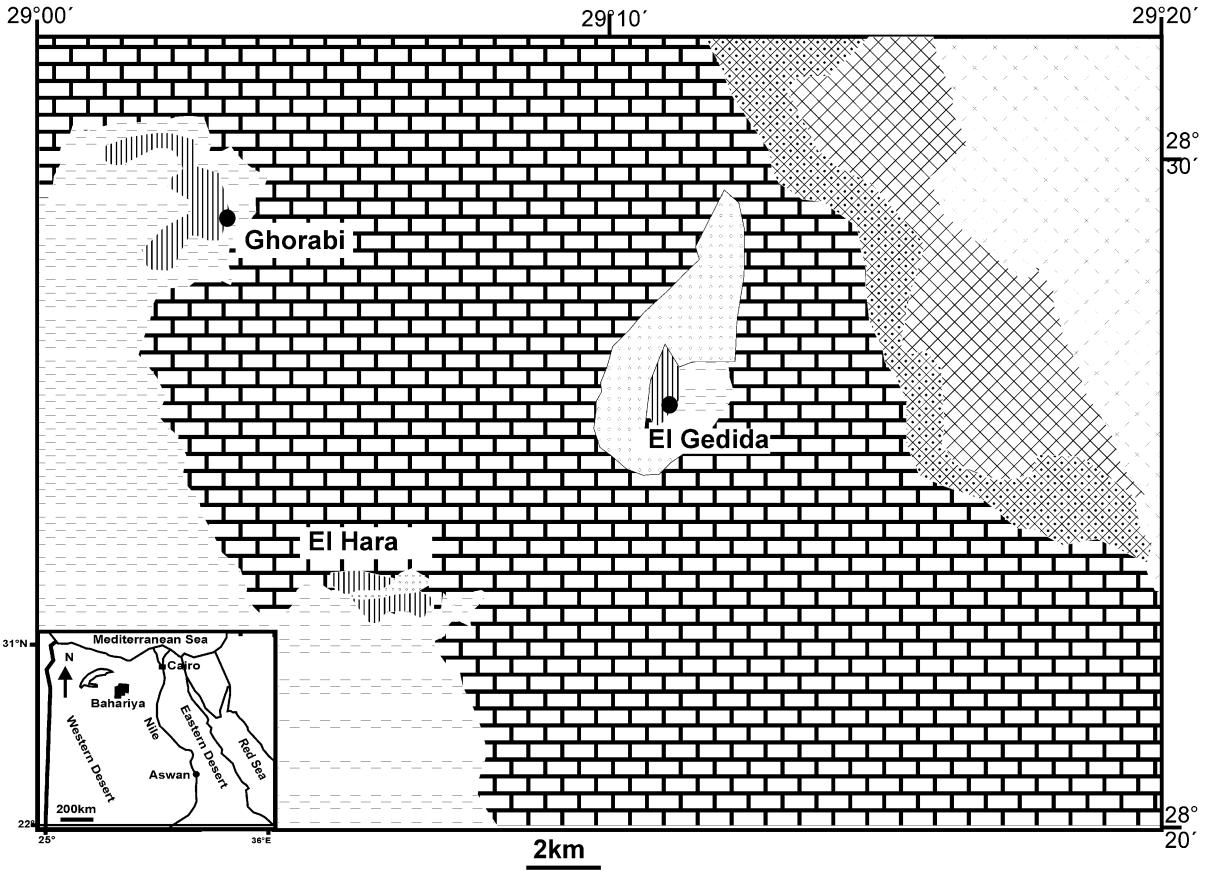

ACCEPTED MANUSCRIPT

Figure 2

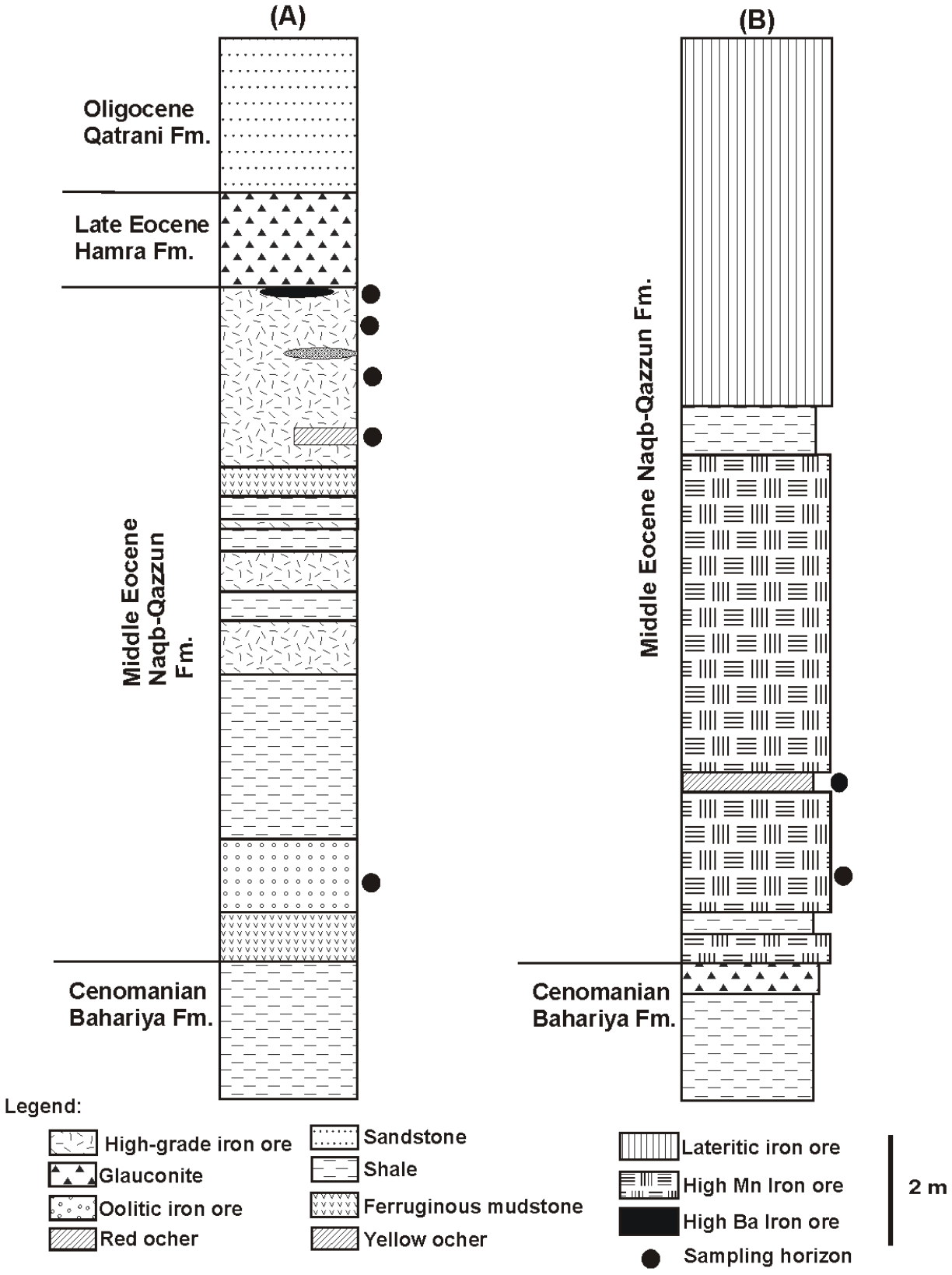

ACCEPTED MANUSCRIPT

Figure 3

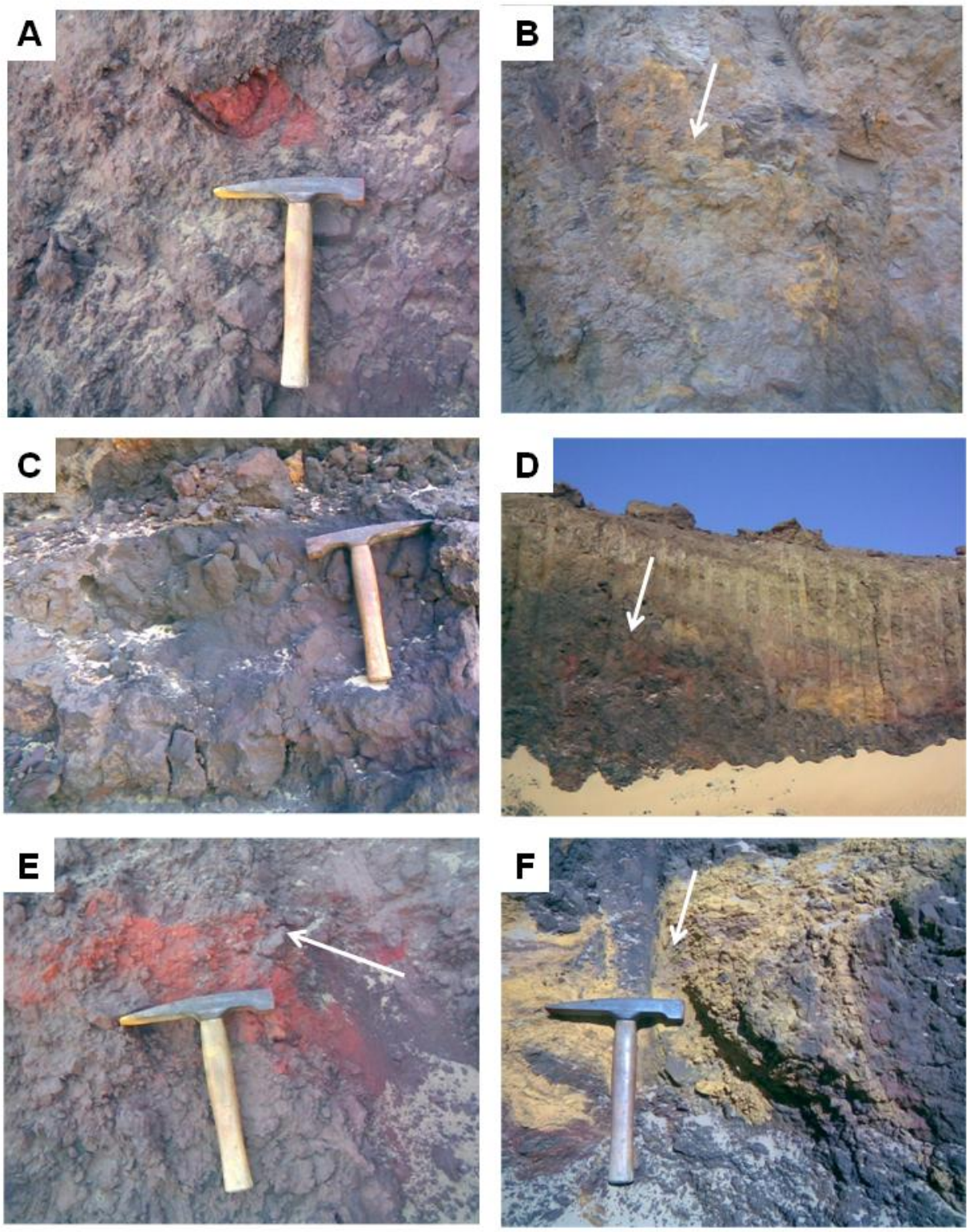

ACCEPTED MANUSCRIPT

Figure 4

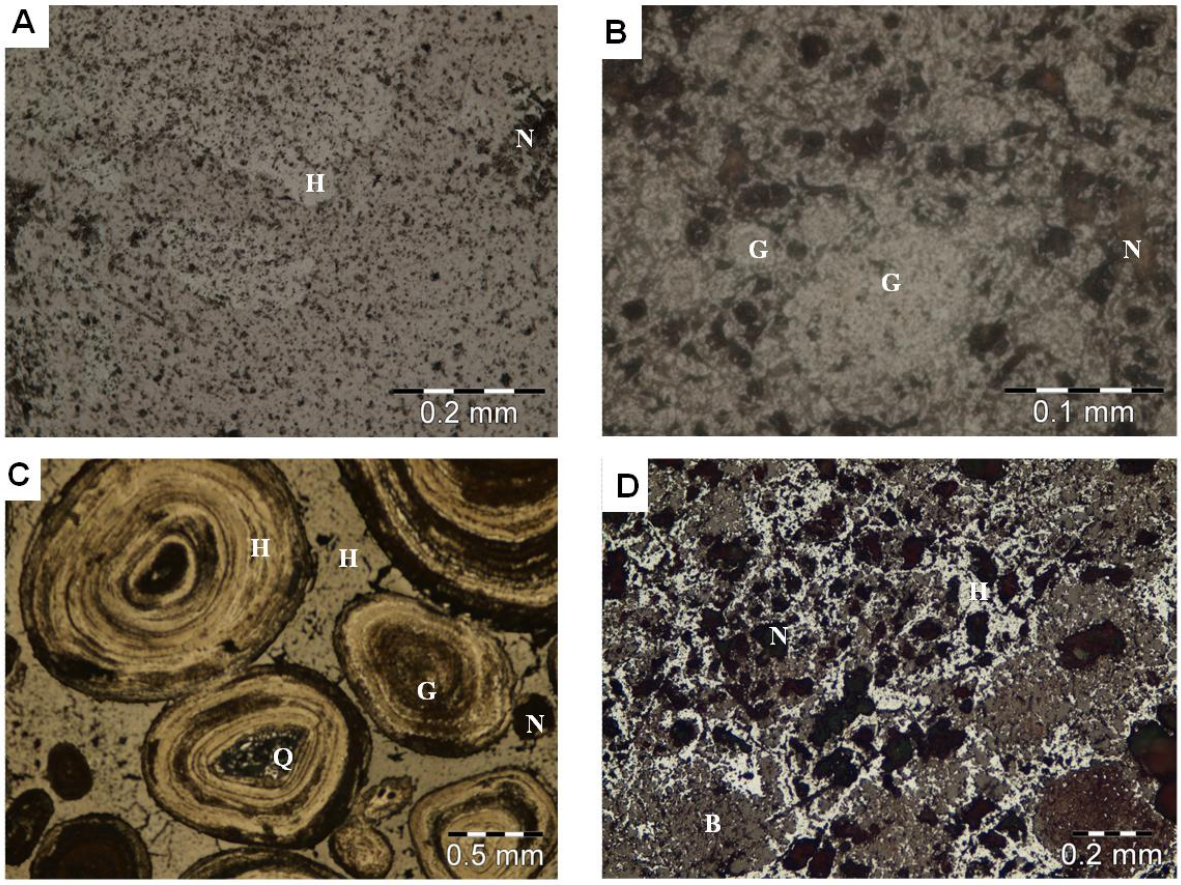

ACCE

ACCEPTED MANUSCRIPT

Figure 5

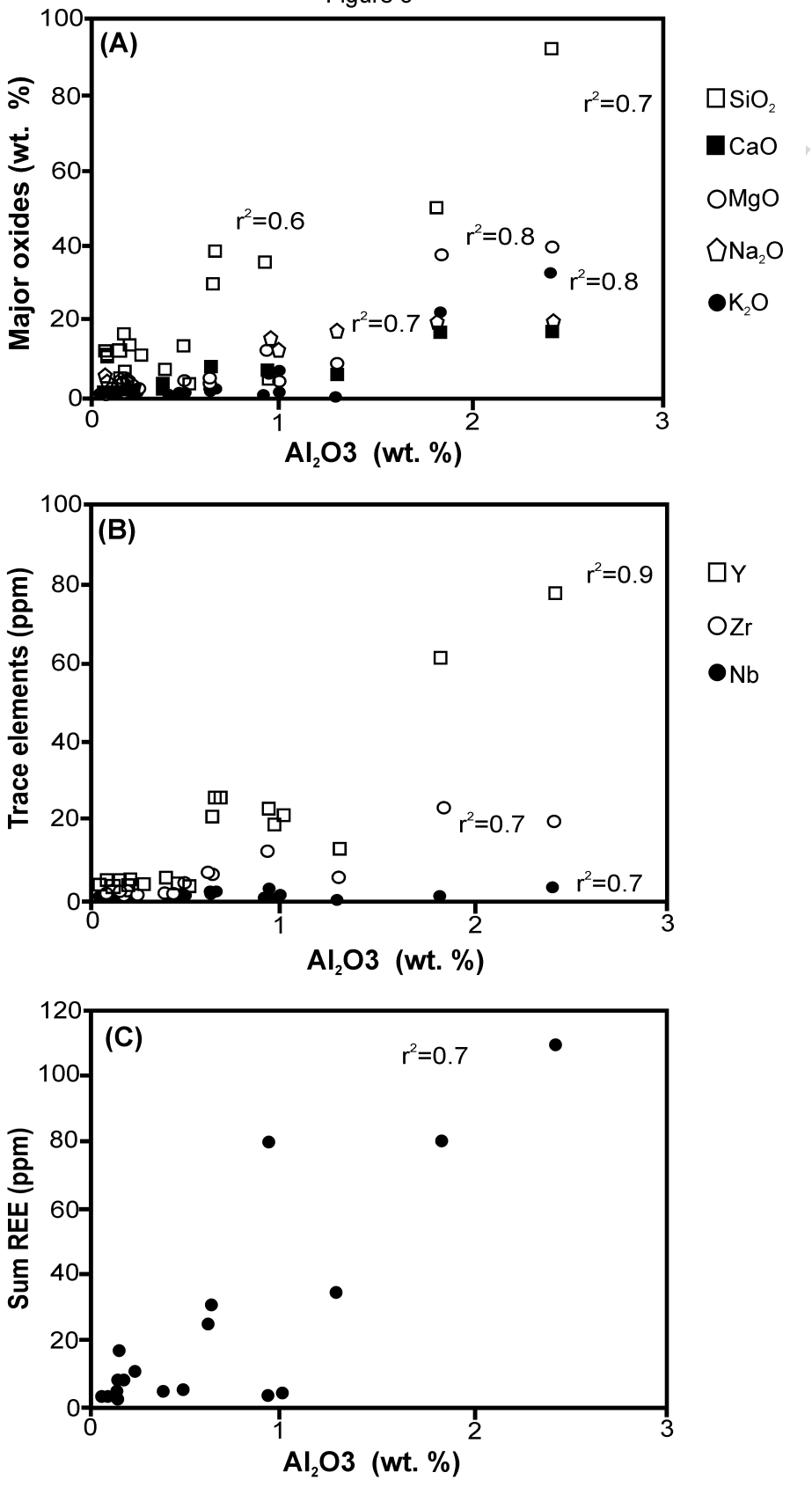

ACCEPTED MANUSCRIPT

Figure 6

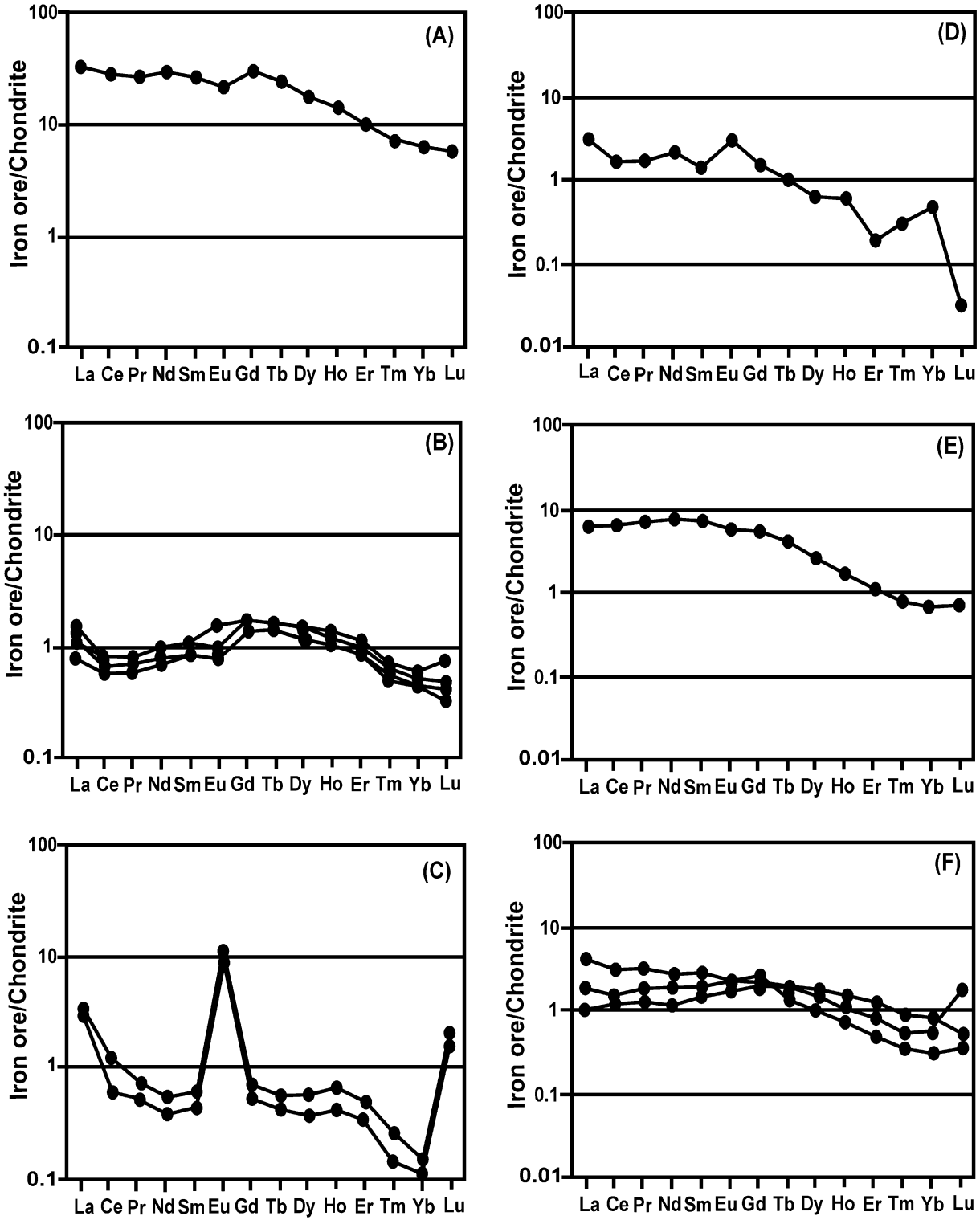

ACCEPTED MANUSCRIPT

Figure 7

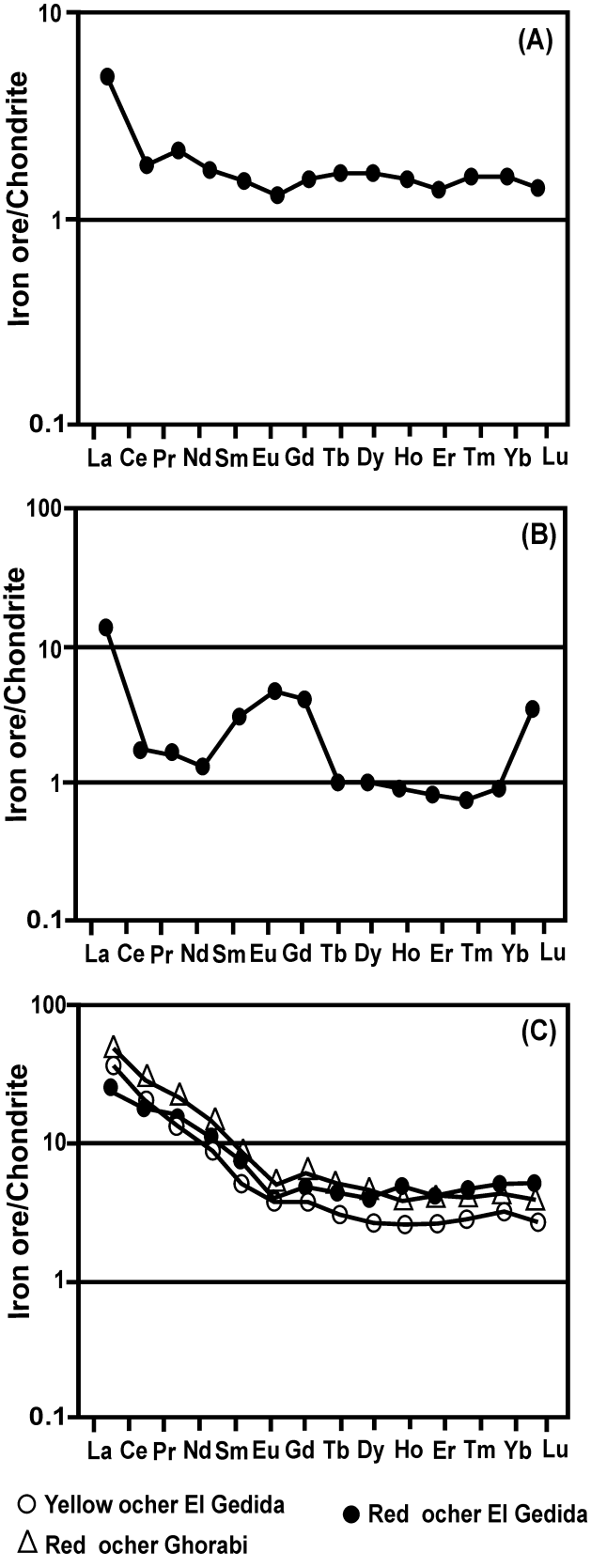

ACCEPTED MANUSCRIPT

Figure 8

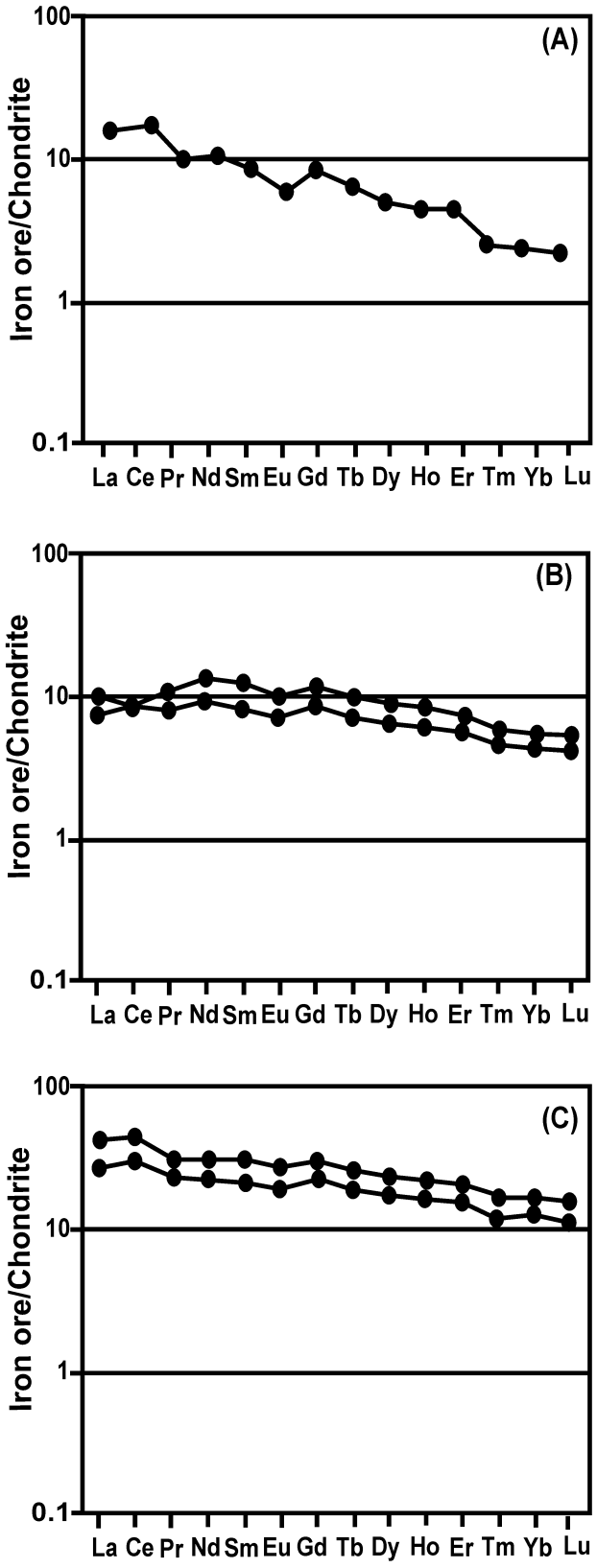

ACCEPTED MANUSCRIPT

Figure 9

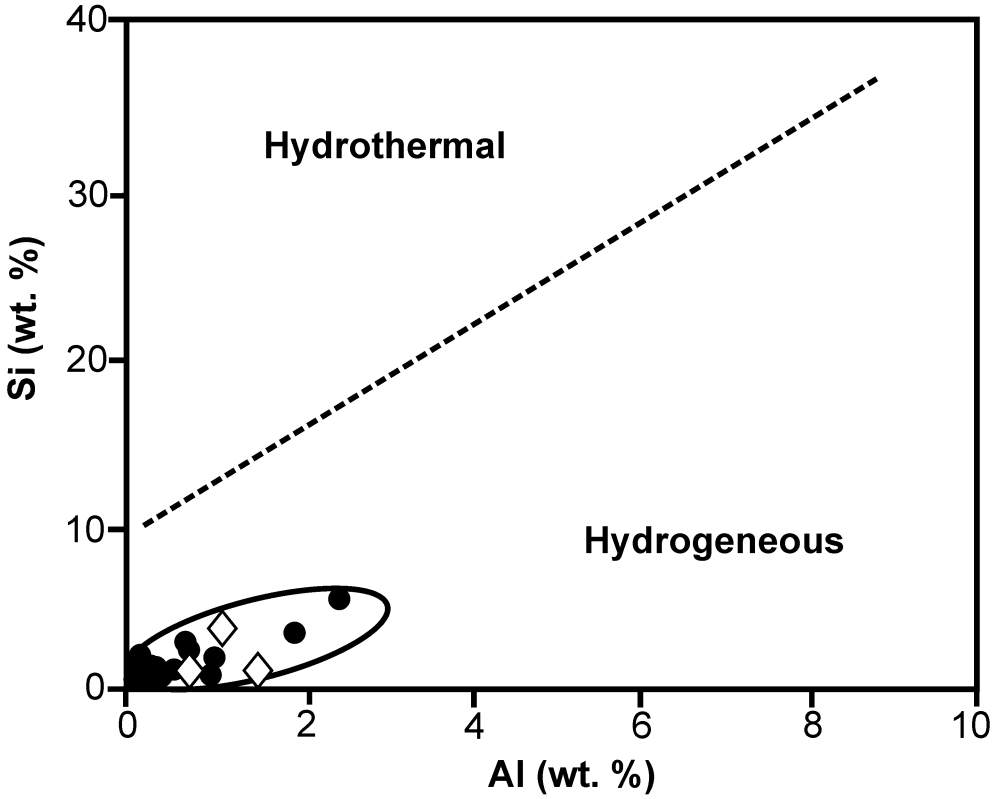

◇ XRF data of bulk ores (this study)

● LA-ICP-MS data of Fe- and Mn- bearing grains (this study)

Field of EPMA data of Fe- and Mn- bearing grains (Baioumy et al., 2012)

ACCEPTED MANUSCRIPT

Figure 10

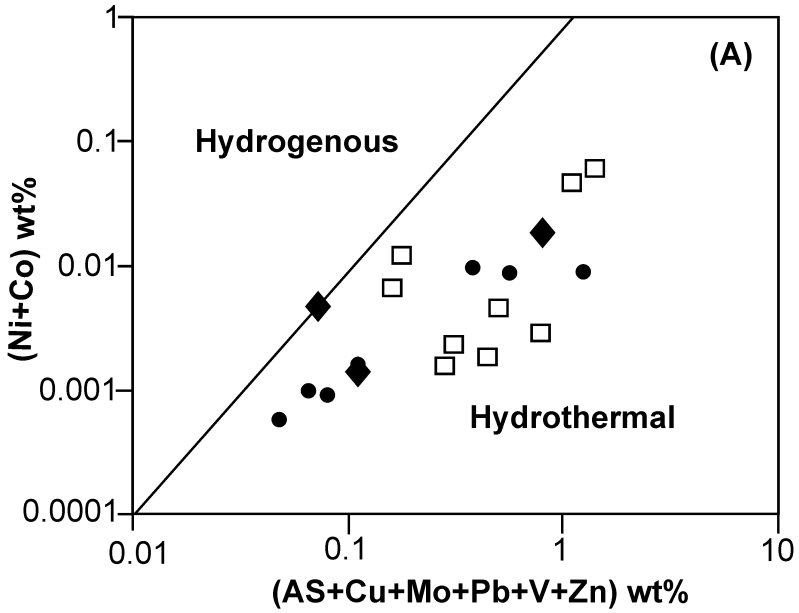

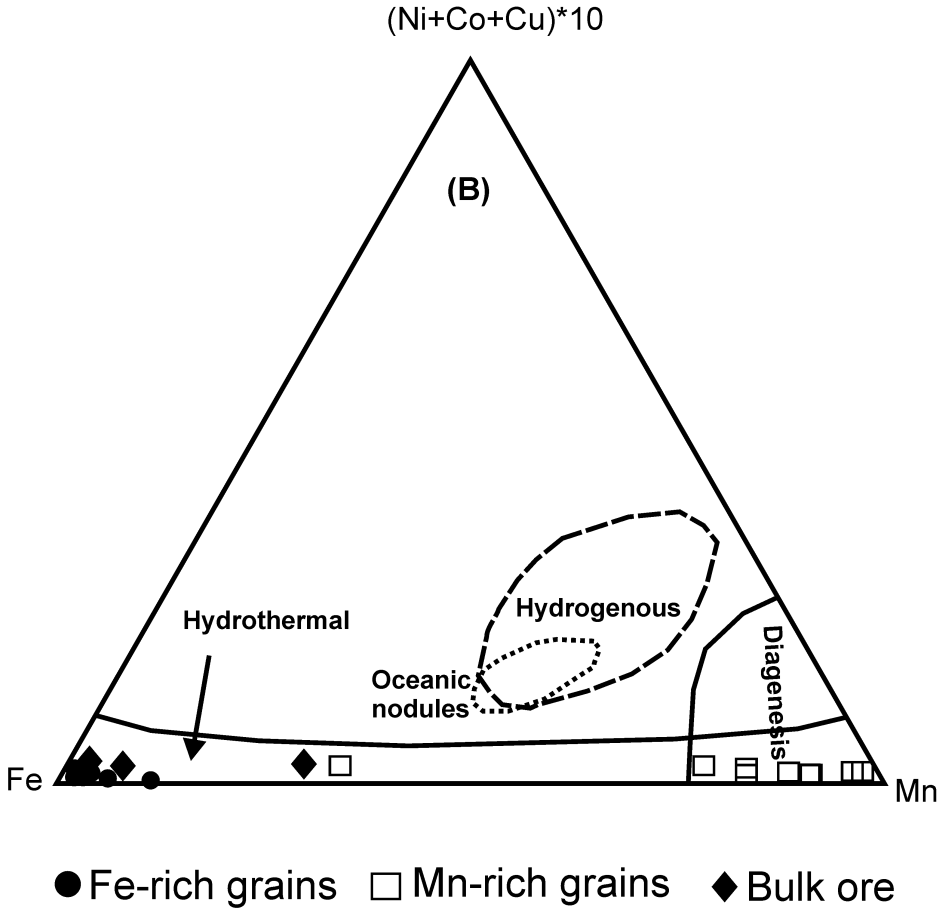

ACCEPTED MANUSCRIPT

Figure 10

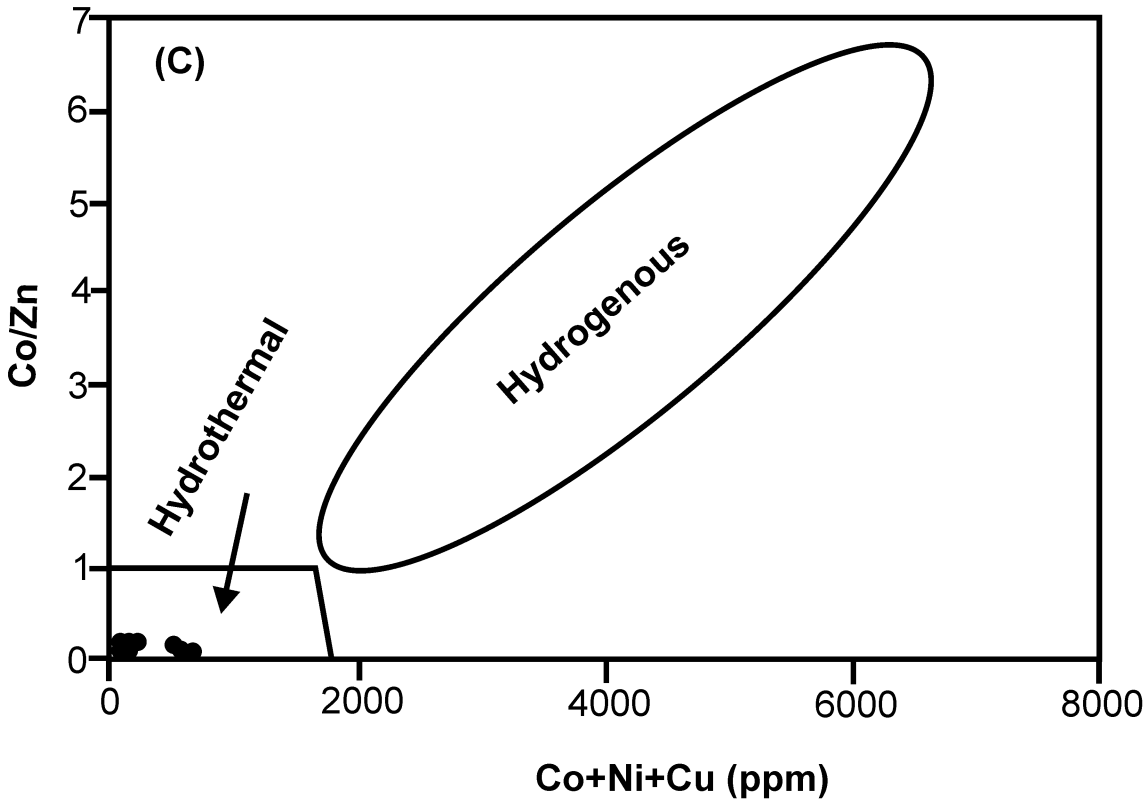

ACCEPTED

ACCEPTED MANUSCRIPT

Table 1: Major oxides (wt. %) in the bulk ores and Fe- and Mn-bearing minerals from the Ghorabi and El Gedida iron ores. Bulk samples were analyzed by X-ray fluorescence (XRF), while mineral grains were analyzed by in situ LA-ICP-MS.

Area	Sample		SiO_2	TiO_2	Al_2O_3	Fe_2O_3	MnO_2	MgO	CaO	Na_2O	K_2O	P_2O_5	L.O.I	Total
El Gedida	14	Bulk	1.84	0.95	0.91	86.7	0.41	bdl	bdl	bdl	bdl	0.05	8.83	99.82
		Mn-bearing minerals	0.26	0.35	0.93	0.22	80.58	0.35	0.37	0.72	0.32		nm	84.12
			0.28	0.33	0.98	0.19	99.13	0.29	0.38	0.63	0.32		nm	82.54
		Fe-bearing minerals	0.65	bdl	0.12	87.97	4.56	0.13	0.10	0.10	bdl		nm	93.59
			0.60	bdl	bdl	90.01	2.03	0.10	0.10	0.29	bdl		nm	93.18
			0.55	bdl	bdl	91.80	2.03	0.10	0.10	0.15	bdl		nm	94.77
			0.49	bdl	bdl	91.37	1.44	0.10	0.10	0.14	bdl		nm	93.70
	15	Bulk	0.71	0.68	0.47	88.55	2.67	bdl	bdl	bdl	bdl	0.05	6.77	100.01
		Mn-bearing minerals	0.36	bdl	0.39	0.90	90.20	0.12	0.21	0.10	bdl		nm	92.35
			0.36	bdl	0.15	0.47	92.47	bdl	0.14	0.10	bdl		nm	93.81
			0.21	bdl	0.14	0.67	92.11	bdl	0.12	0.16	0.32		nm	93.83
		Fe-bearing minerals	0.82	bdl	0.16	86.48	3.80	0.30	0.10	0.10	bdl		nm	91.72
			0.57	bdl	0.24	45.18	49.26	0.12	0.15	0.20	bdl		nm	95.78
			0.69	bdl	0.18	57.38	31.41	0.17	0.11	0.10	bdl		nm	90.06
	Oolitic	Bulk	21.28	bdl	0.51	47.71	0.18	0.45	0.35	1.38	0.12	0.199	28.11	100.51
	High-Ba	Bulk	0.17	2.44	0.38	21.29	0.08	0.07	0.01	0.61	0.14	0.179	75.01	100.61
	Red ocher	Bulk	2.52	0.16	0.24	40.05	0.12	0.57	2.41	1.61	0.10	0.108	52.17	100.11
	Yellow ocher	Bulk	0.62	0.33	0.19	56.06	bdl	0.16	2.57	0.69	0.13	0.582	39.17	100.50
Ghorabi	17	Bulk	bdl	0.32	1.28	47.33	13.91	0.46	0.34	0.84	0.10	0.135	35.33	100.15
		Mn-bearing minerals	2.49	0.15	1.83	3.41	69.59	1.85	0.92	1.03	1.14		nm	82.40
			4.63	0.16	2.41	4.88	66.05	1.99	0.93	0.96	1.64		nm	83.65
		Fe-bearing minerals	1.51	bdl	0.61	77.86	11.43	0.26	0.40	0.16	0.10		nm	92.39
			2.00	bdl	0.63	81.20	8.81	0.27	0.30	0.22	0.10		nm	93.56
	Red ocher	Bulk	13.65	0.33	4.72	68.15	3.58	1.39	0.76	1.02	0.68	0.644	5.09	100.65

ACCEPTED MANUSCRIPT

bdl= below detection limit nm= not measured

Table 2: Trace elements concentrations (ppm) in the bulk ores and Fe- and Mn-bearing minerals from the Ghorabi and El Gedida iron ores. Bulk samples were analyzed by ICP-MS, while mineral grains were analyzed by in situ LA-ICP-MS.

Samples	El Gedida													
	14							15						
	Bulk	Mn-bearing minerals		Fe-bearing minerals				Bulk	Mn-bearing minerals			Fe-bearing minerals		
Li	bdl	30.09	33.73	2.22	bdl	bdl	bdl	bdl	1.15	2.57	1.78	4.28	1.09	1.48
Be	5	2.29	2.77	3.90	3.07	3.35	2.38	bdl	1.12	2.53	2.07	6.03	2.24	2.63
B	bdl	249.26	234.62	54.38	29.65	38.34	71.17	bdl	22.27	35.71	30.80	158.64	54.88	58.14
Sc	bdl	bdl	bdl	0.25	0.18	0.16	0.20	bdl	2.50	5.32	4.81	4.09	2.38	1.17
V	122	0.17	0.26	39.64	41.52	19.23	16.58	31	3.56	6.16	4.56	24.88	28.33	37.24
Cr	bdl	bdl	bdl	55.44	58.93	22.56	21.96	bdl	4.31	2.65	6.65	7.12	4.99	5.13
Co	115.4	30.77	76.04	4.80	0.21	0.52	0.90	4	2.75	9.22	4.68	13.75	3.42	4.47
Ni	48.5	35.96	39.72	10.46	5.61	8.95	8.53	9.5	13.69	21.33	43.82	73.12	14.68	15.35
Cu	14.8	1.03	1.49	0.78	0.34	0.66	1.98	0.6	1.22	5.37	1.48	4.02	2.08	1.15
Zn	7564	1312	1442	951.29	345.38	569.39	712.71	1100	2739	8085	4724	11466	4400	2838
As	3.9	18.21	22.10	61.58	73.88	71.27	49.59	33.7	16.32	169.80	18.78	321.86	97.44	157.24
Rb	11.3	3.55	3.61	0.24	bdl	bdl	bdl	0.7	1.69	0.62	2.35	1.18	0.38	1.01
Sr	620.9	527.63	666.15	42.02	29.84	19.47	19.64	151.6	127.15	313.62	158.79	678.99	276.71	207.17
Y	23.4	18.99	21.60	4.61	2.58	3.13	2.83	1.4	3.74	1.45	5.23	3.03	1.98	1.75
Zr	11.7	bdl	bdl	0.93	0.43	0.41	0.49	1.9	0.37	0.13	0.12	0.77	0.51	0.31
Nb	1.8	bdl	bdl	bdl	bdl	bdl	bdl	bdl	bdl	bdl	bdl	0.11	bdl	bdl
Mo	2.7	253.66	273.81	28.17	8.97	8.86	7.82	13.7	179.65	266.33	248.47	516.01	227.49	162.78
Cs	1	0.25	0.23	bdl	bdl	bdl	bdl	bdl	bdl	bdl	0.05	bdl	bdl	bdl
Ba	209	12382	13187	8743	63.46	67.37	52.63	12102	9704	1221	13154	4451	2859	5589
Hf	0.7	1.36	1.48	0.11	bdl	bdl	bdl	bdl	bdl	bdl	0.15	bdl	bdl	bdl
Ta	bdl	bdl	bdl	bdl	bdl	bdl	bdl	bdl	bdl	bdl	bdl	bdl	bdl	bdl
Pb	6.9	0.58	0.52	1.12	1.50	1.36	0.89	0.3	bdl	0.15	0.12	0.91	0.19	0.31
Th	0.8	0.03	0.01	0.12	0.08	0.08	0.08	bdl	bdl	0.10	bdl	0.21	0.14	0.15
U	11.6	bdl	bdl	2.45	2.69	3.08	2.09	1.60	bdl	2.25	18.45	3.76	2.88	2.14

bdl= below detection limit

ACCEPTED MANUSCRIPT

Table 2: Cont.

Samples	Ghorabi (17)				
	Bulk	Mn-bearing minerals		Fe-bearing minerals	
Li	bdl	26.67	36.37	9.47	11.18
Be	10	5.08	6.05	2.18	2.58
B	bdl	405.68	693.46	59.29	88.26
Sc	bdl	2.55	3.46	1.35	1.75
V	68	55.62	74.46	33.71	47.22
Cr	bdl	16.15	23.98	13.03	17.97
Co	20.1	277.88	341.63	40.91	18.98
Ni	31	201.28	261.28	56.36	69.56
Cu	2.9	16.32	21.52	5.18	4.48
Zn	629	10247	12887	3654	5367
As	8.5	24.94	37.70	10.37	16.48
Rb	2.8	124.00	172.90	15.93	19.20
Sr	218.3	1402	1766	431	502
Y	13.1	61.26	77.55	20.60	26.47
Zr	5.2	23.12	19.46	6.12	5.92
Nb	bdl	2.01	3.04	0.75	1.02
Mo	15.9	323.28	420.40	93.98	115.51
Cs	0.2	7.67	10.77	0.99	1.26
Ba	3227	35296	44012	6746	7380
Hf	bdl	0.87	0.78	0.22	0.22
Ta	bdl	0.13	0.21	0.04	0.07
Pb	1.8	4.48	6.85	1.62	2.36
Th	bdl	1.65	2.25	0.68	0.83
U	2.4	65.44	85.61	24.69	16.33

bdl= below detection limit

ACCEPTED MANUSCRIPT

ACCEPTED MANUSCRIPT

Table 3: Rare earth elements concentrations (ppm) in the bulk ores and Fe- and Mn-bearing minerals from the Ghorabi and El Gedida iron ores. Bulk samples were analyzed by ICP-MS, while mineral grains were analyzed by in situ LA-ICP-MS.

Samples	El Gedida													
	14							15						
	Bulk	Mn-bearing minerals		Fe-bearing minerals				Bulk	Mn-bearing minerals			Fe-bearing minerals		
La	10.1	0.96	1.00	0.43	0.34	0.32	0.26	0.90	0.40	1.28	0.57	1.95	1.05	0.80
Ce	22.8	0.51	0.93	0.59	0.53	0.57	0.47	1.30	1.17	2.41	1.15	5.24	3.05	2.61
Pr	3.31	0.07	0.08	0.09	0.08	0.09	0.07	0.19	0.18	0.38	0.21	0.91	0.52	0.31
Nd	17.5	0.24	0.30	0.53	0.47	0.51	0.43	1.30	0.92	1.68	1.09	4.59	2.73	1.67
Sm	5.05	0.09	0.11	0.20	0.16	0.20	0.16	0.27	0.34	0.51	0.35	1.40	0.87	0.49
Eu	1.6	0.64	0.70	0.11	0.06	0.06	0.06	0.22	0.15	0.15	0.17	0.41	0.26	0.17
Gd	8.01	0.14	0.18	0.41	0.35	0.41	0.36	0.42	0.48	0.59	0.54	1.43	0.89	0.51
Tb	1.17	0.02	0.03	0.07	0.06	0.07	0.06	0.05	0.08	0.08	0.09	0.19	0.13	0.07
Dy	5.53	0.12	0.18	0.45	0.38	0.45	0.38	0.21	0.43	0.38	0.54	0.87	0.56	0.37
Ho	0.99	0.03	0.05	0.08	0.07	0.09	0.08	0.04	0.08	0.06	0.10	0.12	0.08	0.05
Er	2.15	0.08	0.10	0.21	0.17	0.20	0.18	0.04	0.18	0.11	0.24	0.23	0.15	0.11
Tm	0.23	0.00	0.01	0.02	0.02	0.02	0.02	0.01	0.02	0.01	0.03	0.03	0.02	0.01
Yb	1.39	0.02	0.03	0.12	0.09	0.11	0.10	0.10	0.11	0.07	0.17	0.14	0.10	0.07
Lu	0.19	0.06	0.06	0.02	0.01	0.01	0.01	0.01	0.02	0.01	0.03	0.02	0.01	0.01
Sum	80.02	2.98	3.75	3.35	2.80	3.13	2.64	5.05	4.56	7.70	5.29	17.52	10.42	7.26
La/Ce	0.44	1.90	1.08	0.73	0.65	0.57	0.55	0.69	0.34	0.53	0.50	0.37	0.34	0.31
Y/Ho	23.6	657.4	471.4	54.5	35.1	35.8	36.6	35.0	48.5	26.0	52.1	24.5	24.8	33.4
(La/Yb)N	4.90	29.38	25.10	2.47	2.55	1.94	1.75	6.07	2.37	13.15	2.25	9.45	6.99	7.35
Eu/Eu*	0.77	17.71	15.09	1.22	0.73	0.68	0.73	2.00	1.11	0.83	1.16	0.89	0.89	1.01
Ce/Ce*	0.90	0.28	0.49	0.60	0.66	0.72	0.73	0.61	1.05	0.81	0.77	0.96	1.00	1.22

ACCEPTED MANUSCRIPT

Table 3: Cont.

Samples	El Gedida				Ghorabi					
	Oolitic	High-Ba	Red ocher	Yellow ocher	17					Red ocher
	Bulk	Bulk	Bulk	Bulk	Bulk	Mn-bearing minerals		Fe-bearing minerals		Bulk
La	1.62	4.15	8.04	11.39	5.1	8.94	13.67	2.34	3.03	14.76
Ce	1.48	1.34	14.96	15.60	14.4	26.27	37.67	6.84	6.78	23.57
Pr	0.27	0.20	1.74	1.62	1.35	2.81	3.91	0.97	1.27	2.62
Nd	1.02	0.80	6.51	5.34	6.3	14.43	19.45	5.71	7.42	8.54
Sm	0.30	0.61	1.45	0.95	1.61	4.45	5.91	1.54	2.18	1.57
Eu	0.10	0.35	0.27	0.28	0.44	1.56	2.01	0.50	0.67	0.36
Gd	0.40	1.05	1.24	0.98	2.11	6.36	8.01	2.22	2.90	1.44
Tb	0.08	0.05	0.20	0.15	0.3	0.96	1.23	0.34	0.44	0.22
Dy	0.55	0.32	1.32	0.86	1.54	5.87	7.51	2.10	2.65	1.33
Ho	0.11	0.07	0.32	0.18	0.31	1.26	1.56	0.44	0.55	0.28
Er	0.30	0.17	0.82	0.55	0.94	3.46	4.21	1.21	1.42	0.84
Tm	0.05	0.02	0.13	0.09	0.08	0.43	0.53	0.15	0.18	0.13
Yb	0.35	0.20	0.92	0.63	0.48	2.67	3.32	0.94	1.09	0.86
Lu	0.05	0.11	0.15	0.08	0.07	0.39	0.49	0.14	0.16	0.13
Sum	6.69	9.43	38.08	38.70	35.03	79.85	109.47	25.43	30.74	56.66
La/Ce	1.1	3.01	0.53	0.73	0.35	0.34	0.36	0.34	0.45	0.63
Y/Ho	nc	nc	nc	nc	42.3	48.5	49.8	46.6	48.1	nc
$(La/Yb)_N$	3.1	14.3	5.9	12.1	7.16	2.26	2.77	1.68	1.87	11.6
Eu/Eu*	0.83	1.33	0.62	0.88	0.73	0.90	0.89	0.83	0.82	0.73
Ce/Ce*	0.45	0.18	0.88	0.70	1.23	1.19	1.16	1.03	0.79	0.80

nc= not calculated

ACCEPTED MANUSCRIPT

Research Highlights

- A mixed hydrogeneous and hydrothermal source was suggested for Baharyia iron ores
- Low La/Ce, high Y/Ho, and negative Eu anomalies support the hydrogeneous source
- High contents of Ba, Zn, and Mo, low ΣREE, suggest the hydrothermal source
- Submarine weathering of glauconites and detrital Fe could be the source of Fe
- Minerals grains geochemistry is important to understand the origin of iron ores

ACCEPTED MANUSCRIPT